Available on the CMS information server **CMS AN-16-295**

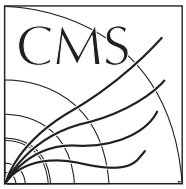

The Compact Muon Solenoid Experiment

CMS Draft Note

Mailing address: CMS CERN, CH-1211 GENEVA 23, Switzerland

2018/04/23
Head Id: 453766
Archive Id: 456752M
Archive Date: 2018/04/02
Archive Tag: trunk

Search for top+photon production in pp collisions at 13 TeV in the muon+jets channel

Seyed Mohsen Etesami and Mojtaba Mohammadi Najafabadi
Institute for Research in Fundamental Sciences (IPM), Tehran, Iran

DRAFT

Abstract

A search is presented for single top quark production in association with a photon in the proton- proton collisions with the CMS detector at the CERN LHC. The analysis is based on a data set corresponding to an integrated luminosity of 35.86 fb^{-1} at the center-of-mass energy of 13 TeV. Events with one muon, a photon, and at least two jets from which exactly one is originating from a b quark are selected. A multivariate analysis based on kinematic and topological properties is used to separate the signal events from backgrounds and the expected signal is extracted using a maximum-likelihood fit to the distribution of the multivariate discriminant defined with boosted decision tree. The obsereved (expected) signal significance is 4.4(3.0) standard deviations and the measured production cross section of $\sigma(t\gamma)\mathcal{B}$ within the kinematic region $E_{T,\gamma} > 25$ GeV, $|\eta| < 1.4442$, and $\Delta R(X,\gamma) > 0.5$ ($X = \mu$,b jet,light jet), is $115 \pm ^{+37}_{-32}$(stat $\oplus$ syst) fb which agrees with the standard model prediction.

This box is only visible in draft mode. Please make sure the values below make sense.

PDFAuthor: S.M.Etesami,M.Mohammadi Najafabadi
PDFTitle: Search for top+photon production at 13 TeV in the muon+jets channel
PDFSubject: CMS
PDFKeywords: CMS, physics, software, computing

Please also verify that the abstract does not use any user defined symbols

DRAFT

1 Introduction

The standard model (SM) of particle physics has been found to be prosperous in explaining the strong and electroweak interactions. However, there are unanswered questions concerning possible SM extensions that incorporate new particles and new interactions. Studying top quark interactions could provide applicable information in probing the extensions of the SM. As a result, precise measurements of the top quark interactions are necessary since any deviation from the SM expectations would be indicative of new physics. For example, new physics effects could show up in the top quark couplings with the electroweak gauge bosons which can be studied directly through single top events with an additional gauge boson such as top+γ and top+Z processes. In particular, single top events in association with a photon provide a test for the structure of $t\bar{t}\gamma$ couplings as well as triple gauge boson couplings [1, 2]. Studying $t\bar{t}\gamma$ coupling is also possible through top quark pair production plus a photon production which has been carried out by several experiments [3–5].

Similar to the single top quark production at the LHC, single top+γ events can be produced in three separate production processes, t-channel, s-channel, and tW-channel. The single top+γ in the t-channel mode is the dominant process in which the involved W-boson is space-like. Representative Feynman diagrams for single top+γ production in the t-channel mode is shown in Fig.1. The s-channel diagrams could be obtained by rotating the t-channel diagram in such a way that the virtual W boson becomes time-like. In the tW-channel process, one of the initial partons is a b quark in the proton sea, as in the t-channel process, and another one is a gluon. The involved W boson in this process, that is produced in the final state, is real, i.e. $q_W^2 = m_W^2$.

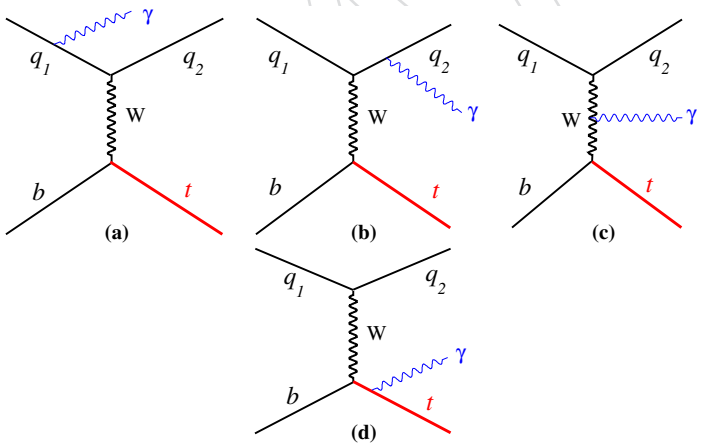

Figure 1: Representative leading order Feynman diagrams for the process of $tj\gamma$ production.

In general, in the top+γ production, the photon radiation can occur in both top quark production and top quark decay. As a result, in top+γ in the t-channel mode the following processes have to be considered:

$$\begin{aligned} pp &\rightarrow tj\gamma,\ t \rightarrow Wb \rightarrow l\nu b, \\ pp &\rightarrow tj,\ t \rightarrow Wb\gamma \rightarrow l\nu b\gamma, \\ pp &\rightarrow tj, t \rightarrow Wb,\ W \rightarrow l\nu\gamma. \end{aligned} \tag{1}$$

The Feynman diagrams contributing to the above first process are depicted in Fig.1. There are additional Feynman diagrams corresponding to the cases that photon is emitted from the W

boson, b-quark and the charged lepton which are presented in Fig.2. In general, we cannot distinguish between the photon emission from top quark production and decay therefore both needs to be considered.

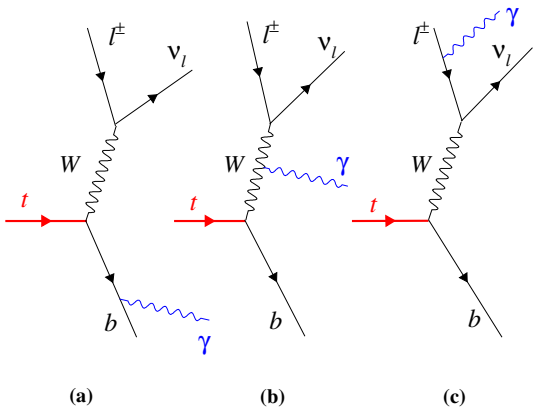

Figure 2: Additional Feynman diagrams contributing to $l\nu b\gamma$ production in proton-proton collisions at the LHC.

The aim of this note is to measure the cross section for the process of single top quark associated with a photon in the t-channel mode, $pp \rightarrow tj\gamma$, using data equivalent to 35.86 fb^{-1} of integrated luminosity at the center-of-mass energy of 13 TeV recorded by the CMS detector in 2016 in muon+jets channel (including muons from the τ-lepton decays).

The general features of the signal are as follows. It has exactly one energetic and well isolated muon from the top quark decay, two energetic jets from which one should originate from the hadronization of a b-quark. Almost similar to the single top t-channel, the light flavor jet tends to reside in the forward/backward region of the detector (high-η region). An isolated photon and missing transverse energy due to undetected neutrino, in the W boson decay, are of the signal characteristics.

2 Data and simulated samples

To calculate the signal (top+γ) efficiency, estimation of the contributions of some of the background processes and to evaluate the effects of systematic uncertainties, Monte Carlo (MC) simulated samples are used. All simulated samples are generated considering multiple proton-proton interactions (pile-up). A re-weighting is performed based on the CMS official recommendation, to match the distribution of the number of interactions per bunch crossing to the one observed in data. The details of the pile-up reweighting will be discussed later. All the MC samples are passed through the GEANT4 package [6] for simulation of detector response using the CMS detector software CMSSW_8_0_25 and the same reconstruction software is applied on data.

2.1 Data sample

In this analysis, we have concentrated on the muonic decay of the W boson in the top quark decays, as a result SingleMuon datasets are used. The list of all datasets used in the analysis

DRAFT

is presented in Table 1. These datasets have been collected with the CMS detector in 2016 at the center-of-mass energy of 13 TeV and are corresponding to the total integrated luminosity of 35.86 fb^{-1}. The integrated luminosity has been calculated using the CMS official tool [7].

Table 1: The list of datasets and their corresponding integrated luminosities used for the analysis.

Dataset	Integrated Luminosity fb^{-1}
SingleMuon/Run2016B_03Feb2017-v2/MINIAOD	5.78
SingleMuon/Run2016C_03Feb2017-v1/MINIAOD	2.57
SingleMuon/Run2016D_03Feb2017-v1/MINIAOD	4.24
SingleMuon/Run2016E_03Feb2017-v1/MINIAOD	4.00
SingleMuon/Run2016F_03Feb2017-v1/MINIAOD	3.10
SingleMuon/Run2016G_03Feb2017-v1/MINIAOD	7.54
SingleMuon/Run2016H_03Feb2017-v2/MINIAOD	8.39
SingleMuon/Run2016H_03Feb2017-v3/MINIAOD	0.21

2.2 Simulation of t-channel top+γ process

Signal events are simulated using MADGRAPH5_AMC@NLO at QCD next-to-leading order (NLO) [8]. Then the top quark is decayed using the MadSpin package interfaced with the MADGRAPH5_AMC@NLO 2.2.2 generator. The NNPDF23 (NLO) [9] is used as the proton parton distribution function and a variable renormalization- and factorization-scale is considered. The top quark mass is set 172.5 GeV. The initial and final state radiation as well as hadronization and decays of unstable particles are simulated using PYTHIA 8 [10] with tune CUETP8M1 [11].

The cross section of the signal process $pp \rightarrow t + j + \gamma$ becomes divergent when the emitted photon is collinear to the initial particle. In order to avoid such divergencies, we impose a minimum cut of 10 GeV on the transverse momentum of the photon.

To quantify the importance of contributions from the additional diagrams appearing in the top quark decays (Fig.2), we compare the cross sections of $pp \rightarrow tj\gamma \times Br(t \rightarrow l\nu b)$ and $pp \rightarrow l\nu b\gamma j$:

$$\frac{\sigma(l\nu bj\gamma)}{\sigma(tj\gamma) \times Br(t \rightarrow l\nu b)}, \tag{2}$$

In Fig.3, the ratio of the cross sections of $\sigma(pp \rightarrow l\nu b\gamma j)$ to $\sigma(pp \rightarrow tj\gamma) \times Br(t \rightarrow l\nu b)$ is shown as a function of cut on the photon transverse momentum. We observe that the new diagrams where the photon is emitted from the top quark decay products has a few percent contributions when the photon transverse momentum cut is below 35 GeV. The relative size of the new contributions depends on the minimum cut on the photon transverse momentum. The quick decrease is due to the suppression of the amplitudes in Fig.2 for increasing photon transverse momentum.

This calculation is performed with CompHEP event generator [12]. It calculates the matrix element of each process and it has the ability of obtaining the contribution of each sub-process separately.

The ratio presented in Fig. 3 has been calculated at parton level after applying standard cuts on the final state particles. The transverse momenta of b-quark and light quark are required to be greater than 30 GeV with $|\eta_b| < 2.5$ and $|\eta| < 5.0$. The lepton transverse momentum has been

DRAFT

required to be larger than 20 GeV and $|\eta| < 2.5$. The angular separation between every two particles also has been required to be $\Delta R(i,j) = \sqrt{(\eta_i - \eta_j)^2 + (\phi_i - \phi_j)^2} > 0.5$. As it can be seen, including the photon radiations from top quark decay products, i.e. the contributions of diagrams presented in Fig.2, leads to 0.02 increase on the cross section when the cut on photon transverse momentum is 25 GeV and the effects of new diagrams disappear when we go to larger cut on photon p_T. The other reasons for applying these cuts are presented in Sec.4.4.

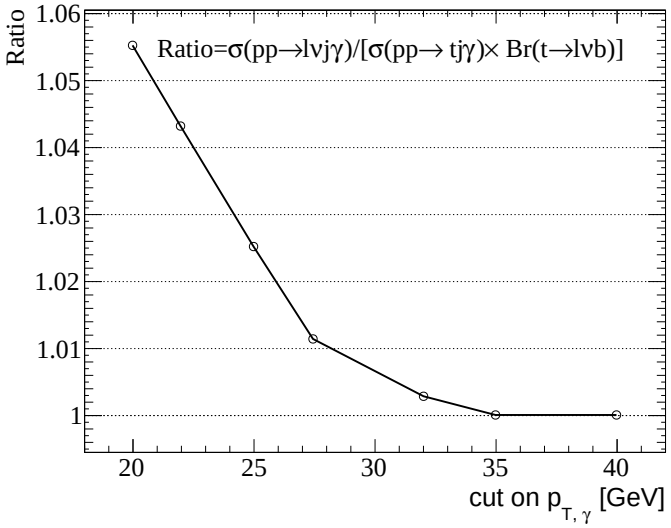

Figure 3: The ratio of $\sigma(pp \to l\nu b\gamma j)$ to $\sigma(p \to tj\gamma) \times Br(t \to l\nu b)$ as a function of cut on the photon transverse momentum.

The photons from showering prefer to be emitted collinear to the charged lepton, light- and b-quark in the final state. Applying cuts on $\Delta R(\gamma, l)$, $\Delta R(\gamma, b)$, and $\Delta R(\gamma, q)$ help remove a significant part of the overlap between single top t-channel process and the signal process. For more illustration, we present the generator level distributions of $\Delta R(\gamma, l)$, $\Delta R(\gamma, b)$, and $\Delta R(\gamma, q)$ in Fig.4 which confirm that requiring a minimum cut on the angular separation would remove a large fraction of the single top quark events whose photons are emitted in the showering process and indeed have overlap with the signal process.

2.3 Backgrounds

The background processes can be categorized into two classes of real and fake photons. The first type of backgrounds are the processes with a real photon radiated either from initial state or final state partons (ISR, FSR) and from the intermediate states. The second type of the backgrounds is the one coming from mis-reconstructed photons (fake-photons).
In order to estimate the contribution of the first type of background, we rely on both MC simulated samples and data-driven methods. In particular, the $t\bar{t}$+γ which is the main background is estimated from data and the rest are derived based on MC simulated samples.

For those background processes which we take from simulation, the correct treatment is to estimate the contribution of the samples with real photon either come from matrix element (such as $t\bar{t}$+γ, Z+γ+jets, WWγ, ...) or showering ($t\bar{t}$, Z+jets, WW,...) after removing the possible overlaps.

DRAFT

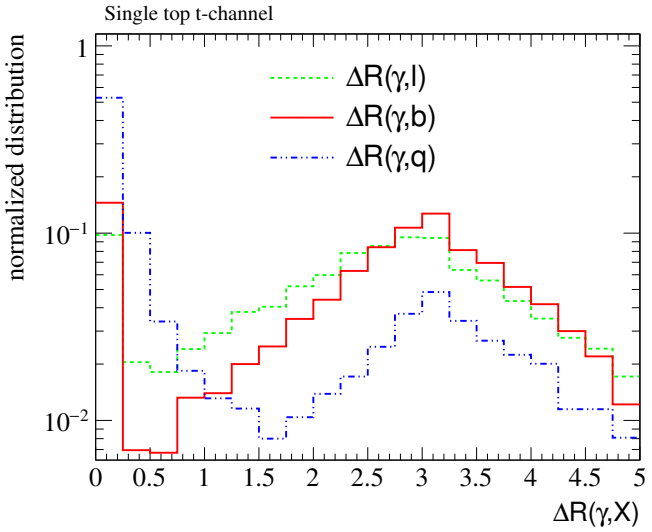

Figure 4: The generator level distributions of $\Delta R(\gamma, l)$, $\Delta R(\gamma, b)$, and $\Delta R(\gamma, q)$ for the single top quark production in the t-channel mode in which the photons are emitted in the showering process.

The contribution of background events with prompt photon from the matrix element is directly taken from simulation. The remaining background contamination with prompt photon appearing the showering process is predicted by matching the reconstructed photon with the photon at generator level. The matching criteria are as follows:

- $\Delta R(\gamma_{rec}, \gamma_{gen}) < 0.3$,
- $\frac{\Delta p_T(\gamma_{rec}, \gamma_{gen})}{p_T} < 1.0$,
- Generator photon mother is required to quarks, leptons, bosons.

In both signal and background processes, there is an overlap between the phase space of emitted photons from matrix element and from showering which needs to be determined and removed. As it has been mentioned before, the photons from showering prefer to be emitted collinear with its mother. Therefore, applying lower cuts on $\Delta R(\gamma, X)$, $X = \mu$,jets, reduce a significant part of the overlap in the photon phase space and rest is removed in the analysis.

In this analysis, top pair, single top t-channel and tW-channel events are generated at NLO using the POWHEG [13] generator. W+γ+jets, Z+γ+jets, W+jets and single top s-channel productions are simulated with aMC@NLO generator. Diboson events (WW, WZ and ZZ) are simulated using PYTHIA 8 at leading order. The parton shower, hadronization and the underlying event are added using PYTHIA 8 generator. The datasets names of the background processes and their related cross sections are presented in Table 2. The **RunIISummer16MiniAODv2** MC samples from the official CMS production are used in the analysis.

3 Trigger

In the muon channel of top quark decay, we select events if they pass either the `HLT_IsoMu24` or the `HLT_IsoTkMu24` trigger paths in both data and MC. These trigger paths require the

Table 2: Datasets names of the signal and background samples used in the analysis.

Dataset	Cross-section [pb]
TGJets_TuneCUETP8M1_13TeV_amcatnlo_madspin_pythia8	2.97 (NLO)
TTGJets_TuneCUETP8M1_13TeV-amcatnloFXFX-madspin-pythia8	3.70 (NLO)
TT_TuneCUETP8M1_13TeV-powheg-pythia8	831.76 (NNLO)
ST_t-channel_top_4f_leptonDecays_13TeV-powheg-pythia8_TuneCUETP8M1	44.33 (NLO)
ST_t-channel_antitop_4f_leptonDecays_13TeV-powheg-pythia8_TuneCUETP8M1	26.38 (NLO)
ST_s-channel_4f_leptonDecays_13TeV-amcatnlo-pythia8_TuneCUETP8M1	3.36 (NLO)
ST_tW_top_5f_inclusiveDecays_13TeV-powheg-pythia8_TuneCUETP8M1	35.6 (NNLO)
ST_tW_antitop_5f_inclusiveDecays_13TeV-powheg-pythia8_TuneCUETP8M1	35.6 (NNLO)
WJetsToLNu_TuneCUETP8M1_13TeV-amcatnloFXFX-pythia8	61526.7(NNLO)
WJetsToLNu_Pt-100To250_TuneCUETP8M1_13TeV-amcatnloFXFX-pythia8	676.3 (NLO)
WJetsToLNu_Pt-250To400_TuneCUETP8M1_13TeV-amcatnloFXFX-pythia8	23.94 (NLO)
WJetsToLNu_Pt-400To600_TuneCUETP8M1_13TeV-amcatnloFXFX-pythia8	3.03 (NLO)
DYJetsToLL_M-10to50_TuneCUETP8M1_13TeV-amcatnloFXFX-pythia8	18610 (NLO)
DYJetsToLL_M-50_TuneCUETP8M1_13TeV-amcatnloFXFX-pythia8	5943.2 (NLO)
WGToLNuG_TuneCUETP8M1_13TeV-madgraphMLM-pythia8	489 (NLO)
ZGTo2LG_TuneCUETP8M1_13TeV-amcatnloFXFX-pythia8	117.86 (NLO)
WWG_TuneCUETP8M1_13TeV-amcatnlo-pythia8	0.215 (NLO)
WW_TuneCUETP8M1_13TeV-pythia8	63.21 (LO)
WZ_TuneCUETP8M1_13TeV-pythia8	47.13 (NLO)
ZZ_TuneCUETP8M1_13TeV-pythia8	16.523 (NLO)

presence of one isolated online muon candidate with $p_{\mathrm{T}} > 24$ GeV. The trigger efficiencies in simulation are corrected using data-to-MC scale factors which have been obtained from a Tag and Probe method. If an event passes any of the recommended high level triggers, the event is considered for the rest of selection which will be presented in section 4.

4 Physics object reconstruction and selection

A cartoon displaying the single top plus a photon decay process is illustrated in Figure 5. As it can be seen, the final state topology is characterized by the presence of exactly one isolated photon, only an isolated muon, a b-jet from the top quark decay, and a light flavor jet produced in the forward/backward region.
In the following, we describe the definitions of the physics object and selection criteria to find the expected signal events.

4.1 Primary vertex and filter

Before physics object selection and further analysis, events are required to pass several filter steps. These include:

- Well reconstructed primary vertex with $|z| < 24$ cm, $\rho < 2$ cm, where z and ρ are the respective longitudinal and transverse distances of the primary vertex relative to the center of the detector.
- Global Tight Halo 2016 Filter.
- HBHE noise filter.
- HBHE noise Iso filter.

DRAFT

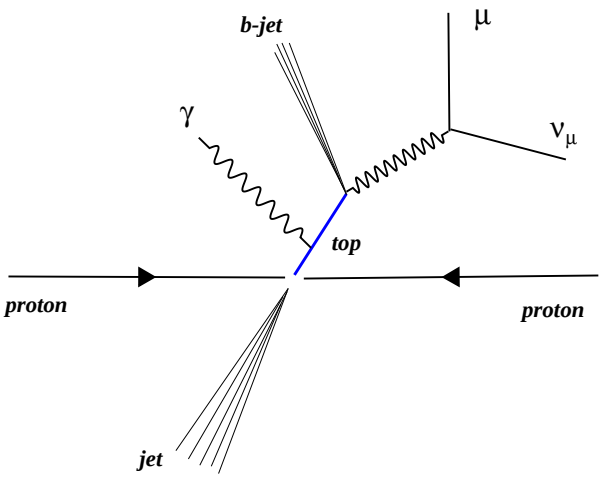

Figure 5: Single top quark plus a photon topology with muonic decay of the top quark.

- EcalDeadCellTriggerPrimitiveFilter.
- Bad PF Muon Filter.
- Bad Charged Hadron Filter.
- EE Bad SC Noise Filter.

For primary vertex reconstruction, all associated tracks have to be compatible with the beam spot in the (x, y) plane. The vertex with highest $\sum p_T^2$ of the associated tracks is selected as the primary vertex.

4.2 Physics object definition and selection

This Section is dedicated to present the physics objects definition, reconstruction and selection. All objects are reconstructed using the PF algorithm [14].

4.2.1 Photon

Photon candidates are reconstructed using clusters of the energy deposits in the electromagnetic calorimeter (ECAL) and merged into superclusters. The PF reconstruction algorithm starts from seeds selection step. Seeds are required to have more energy than its neighbours and an energy greater than a given threshold. The reconstruction algorithm of photon clusters provides the possibility to almost a complete recovery of the photons energy that convert because of the material in front of the ECAL. A detailed description of the algorithm can be found in Ref. [15]. In order to achieve the best photon energy resolution, the ECAL signals are calibrated and corrected for several detector effects. The variation of the crystal transparency during the run is corrected with a dedicated monitoring system and the single-channel response equalized using collision events.
In this analysis, a cut-based photon identification in the "tight ID" working point [15] recommended by the egamma POG for Run 2 analyses is used for photon identification and reconstruction. A short description of the variables used in the analysis for photon identification and isolation is given below.

DRAFT

- H/E : The ratio of the hadronic energy to the ECAL supercluster energy within a cone with radius ΔR = 0.15.
- $\sigma_{i\eta i\eta}$: Shower shape of the electromagnetic cluster computed with logarithmic weights as:

$$\sigma^2_{i\eta i\eta} = \frac{\sum_i^{5\times5} w_i(\eta_i - \bar{\eta}_{5\times5})^2}{\sum_i^{5\times5} w_i},\ w_i = max(0, 4.7 + ln\frac{E_i}{E_{5\times5}}) \quad (3)$$

  where $E_{5\times5}$ and $\bar{\eta}_{5\times5}$ are the energy and the pseudorapidity of the entire 5×5 cluster and E_i and η_i are the energy and pseudorapidity of the ith crystal within 5×5 electromagnetic cluster.
- ρ *corrected PF Photon Isolation*: transverse energy sum associated with all particles identified as photons by the PF algorithm falling inside a cone size $R = 0.3$ around the photon candidate direction with ρ correction applied.
- ρ *corrected PF charged Hadron Isolation*: The p_T of all the PF candidates tagged as charged hadron in a cone of $\Delta R = 0.3$ are summed with pileup ρ correction is applied. A geometric veto with $\Delta R > 0.02$ in barrel and endcap is applied. The charged hadron must be within 0.2 cm along the beam direction and within 0.1 cm transverse to the beam direction of the selected vertex for which the sum is defined.
- *PF neutral hadron isolation*: The p_T of all the PF candidates tagged as neutral hadron in a cone of $\Delta R = 0.3$ are summed with no geometric veto.
- *Electron veto*: A conversion-safe electron veto is applied to avoid misidentifying an electron as a photon. It excludes the photon if there is a gsf-electron matching to the photon supercluster, with no missing hits and having no matching reconstructed conversion.
- *Pixel seed veto*: To ensure that there is no track seed identified in the pixel detector, a pixel seed veto cut is applied.

In this analysis, exactly one photon with transverse energy greater than 25 GeV within pseudorapidity range $|\eta| < 1.4442$ is required. The cut on the photon E_T is in particular useful to suppress a lot of low energy fake photons and photons originating from vertices except the primary vertex. The photons in the endcap region $1.556 < |\eta| < 2.4$ are not considered in the analysis as there is a large photon misidentification rate in this region. The photon candidate is required to not have a track seed in the pixel detector (electron veto). The H/E or fraction of energy deposited in HCAL towers behind the associated electromagnetic energy has to be less than 0.0269. The shower shape width $\sigma_{i\eta i\eta}$ is required to be less than 0.00994 and the charged hadron isolation (after pileup correction) should be less than 0.202. Neutral hadron isolation with ρ correction is required to be less than $0.264 + 0.0148 \times p_T + 0.000017 \times p_T^2$ and the pileup corrected photon isolation should be less than $2.362 + 0.0047 \times p_T$. Photon selection criteria are summarized in Table 3.

4.2.2 Muons

Events are required to have a reconstructed muon with a transverse momentum p_{T} >26 GeV within the pseudorapidity range of $|\eta| < 2.4$. In addition, the reconstructed muon is required to be a global muon and must meet more muon quality requirements which are referred to as tight muon ID [16].

In particular, in order to guarantee a good transverse momentum measurement, muon candidates are required to have at least five valid hits in the silicon tracker, out of which at least one

DRAFT

Table 3: Photon selection criteria [15].

Variable	Selection
p_T	> 25 GeV
η	< 1.4442 (Barrel)
H/E	< 0.0269
$\sigma_{i\eta i\eta}$	< 0.00994
Charged Hadron Iso.	< 0.202
Neutral Hadron Iso.	$< 0.264 + 0.0148 \times p_T + 0.000017 \times p_T^2$
Photon Iso.	$< 2.362 + 0.0047 \times p_T$
Conversion safe electron veto	Applied
Pixel seed veto	Applied

in the pixel detector. Also, this would help for further suppression of muons coming from decays in flight. Muon candidates must have $\chi^2/\text{ndf} < 10$ and at least one valid hit in the muon chambers and at least two segments must match the global muon object in the muon chambers, which suppresses accidental track-to-segment matches. The absolute transverse impact parameter has to be smaller than 0.2 cm w.r.t. the center of the beam spot position. This is useful to suppress the background comes from cosmic ray muons, while the longitudinal distance of the muon track relative to the leading primary vertex must be less than 0.5 cm at the point of the closest approach.

A particle flow (relative) isolation (I_{rel}) with DeltaBeta correction is defined as

$$I_{\text{rel}} = \frac{I^{\text{ch. h}} + max((I^{\gamma} + I^{\text{n. h}} - I^{\text{PU}}), 0)}{p_{\text{T}}}, \tag{4}$$

where $I^{\text{ch. h}}$, I^{γ}, and $I^{\text{n. h}}$ are defined as sum of the transverse energies deposited by stable particles such as photons, charged hadrons and neutral hadrons, respectively, in a cone with a size $\Delta R = 0.4$ around the reconstructed muon direction. In Eq. 4, $I^{\text{PU}} \equiv \Delta\beta \times \sum p_T^{PU} \equiv 0.5 \times \sum p_T^{PU}$ is defined as the sum of p_T of tracks associated to pileup vertices. The $\Delta\beta$ corresponds to the expected neutral contribution to the charge particle in the isolation cone from the observed PU. The muon candidate is required to pass the isolation criteria $I_{\text{rel}} < 0.15$.

In order to take into account the differences in efficiencies between data and simulation, the data-to-MC correction factors for muon are obtained using a Tag and Probe method and are applied to simulated events.

Loose muon veto: Finally, for the sake of reducing contribution of background processes with more than one charged muon like WW, top pair (in dilepton channel), ZZ etc., events containing an additional charged loose muon are discarded. In particular, any event with a further muon with $p_{\text{T}} > 15$ GeV within $|\eta| < 2.4$, satisfying the global muon criteria passing $I_{\text{rel}} < 0.25$, is rejected.

4.2.3 Veto electrons

In order to suppress backgrounds which contain electrons in the final state, any event which contains an electron passing "Veto ID" working point [17] is discarded. Electrons are reconstructed from a cluster in the ECAL and a single track pointing towards this cluster. The electron isolation is based on photons, neutral hadrons, and charged hadrons as identified by the PF algorithm in a cone of $\Delta R < 0.3$ around the electron. Events containing one or more "Veto ID" electron(s) are rejected. The selection criteria for "Veto ID" electron is based on the **eGamma** recommendation and are presented in Table 4.

DRAFT

Table 4: "Veto ID" electron selection criteria.

Variable	Selection ($\lvert\eta_{SC}\rvert < 1.479$)	Selection ($\lvert\eta_{SC}\rvert > 1.479$)
p_T	> 20 GeV	20 GeV
H/E	< 0.356	< 0.211
$\sigma_{i\eta i\eta}$	< 0.0115	< 0.037
$\lvert\Delta\eta\rvert$ in seed	$<$0.00749	< 0.00895
$\lvert\Delta\phi\rvert$ in seed	< 0.228	< 0.213
Rel. comb. PF Iso with EA correction	0.175	0.159
$\lvert\frac{1}{E} - \frac{1}{p}\rvert$	< 0.299	< 0.15
Expected missing inner hits	≤ 2	≤ 3
Pass conversion veto	Applied	Applied

4.2.4 Jets

The reconstructed PF objects are clustered into jets by the anti-k_T algorithm [18] using a distance parameter of 0.4. The jets reconstruction procedure is performed after rejecting charged hadrons associated to a pileup primary vertex. The selection criteria for jet candidates include L1Fastjet corrections compatible with PFnoPU, Level 2 and Level 3 jet energy corrections and L2L3Residual corrections for data. The latest set of JECs (Summer16_23Sep2016V3_MC and Summer16_ 23Sep2016V3_DATA) are applied. In order to have compatible jet energy resolution for Data and MC, we smear energy of jets in MC samples according to the recommendation of JETMET POG[19]. The latest scales factors is taken from Spring16_25nsV10 tag. We apply a jet lepton cleaning in which the charged leptons are removed from the jet collection by requiring a minimum separation of $\Delta R(lepton, jets) > 0.3$.
Furthermore, jets with transverse momenta greater than 40 GeV within $|\eta| < 4.7$ are considered in the analysis. Standard identification criteria are applied to the jets to remove instrumental noise and jets originating from isolated particles. For PF jets official selection cuts correspond to "Loose" Jet Id [20] is used.

4.2.5 b-tagging

Jets originating from hadronization of b-quarks in the top quark decays are identified using CSVv2 b-tagging algorithm [21]. The CSVv2 algorithm uses track and secondary vertices information inside the jet to provide a MVA discriminator for b jet identification. For this study we use the CSVv2 algorithm at the "medium" working point [22] corresponding to a threshold set to 0.8484 as recommended by the the b-tagging Physics Object Group. This working point is optimized based on the best sensitivity which one could achieve for this signal and will be discussed in the section 4.5.

Events are required to have at lease two jets from which only one jet has to pass the medium threshold of the discriminator. To account for differences in the modelling between data and simulation the recommended b-tag and mistag scale factors are applied.

4.2.6 Missing transverse energy

Missing transverse energy is particle flow based and is defined as the opposite of the vectorial sum of the transverse momenta of the identified PF-particles. Data-driven corrections of energy offset are applied to the missing transverse energy. In this analysis, missing transverse energy is required to be greater than 30 GeV. This requirement is useful to suppress the contribution of background processes with no W boson in the final state.

DRAFT

4.3 Top quark reconstruction

The full kinematic of the top quark can be reconstructed from its decay products. All decay products (charged lepton and b-jet) are reconstructed in the detector except the neutrino which remains unobserved. The transverse momentum of the neutrino is assumed to be equal to the missing transverse energy and its longitudinal momentum component ($p_{z,\nu}$) is derived using the W boson mass constraint according to the following relation:

$$m_{\mathrm{W}}^2 = (E_\ell + \sqrt{\not{E}_{\mathrm{T}}{}^2 + p_{z,\nu}^2})^2 - (\vec{p}_{T,\ell} + \vec{\not{E}}_{\mathrm{T}})^2 - (p_{z,\ell} + p_{z,\nu})^2 \,. \tag{5}$$

In general, this quadratic equation has two solutions. In the case of having two real solutions for $p_{z,\nu}$, (which occurs in around 64% of the cases), the solution with the smallest absolute value is chosen. Due to limited $\not{E}_{\mathrm{T}}$ resolution, in some cases the solutions are complex in which only the real part is taken as the $p_{z,\nu}$.

4.4 Other requirements

At the end of event selection, a minimum distance cut in the η, ϕ plane is applied to efficiently reject final state radiation photons, that are emitted from either the final state partons or from the high-p_T muon:

$$\Delta R(\mu, \gamma) > 0.5 \,,\ \Delta R(jets, \gamma) > 0.5. \tag{6}$$

These requirements also help avoid distortion of the photon energy measurement due to the presence of close-by jets. These cuts also reduce the contributions of photons emitted from top quark decay products.

4.5 Optimization of b-tagging WP

As it was mentioned in the section 4.2.5, one should optimize the b-tagging working point and adopt the one which gives the best sensitivity. The criteria for this optimization is the best expected significance which one can obtain from simulation without applying any systematic uncertainties. In order to do that we apply all the requirements mentioned in the previous sections on different objects and consider three b-tagging working points separately. We found the expected significances 2.8σ, 3.1σ and 2.7σ corresponding to the Loose, Medium and Tight WPs, respectively. Therefore, we select the medium WP as the optimized WP for this analysis. Table 5 shows the expected contributions of different SM processes for the three b-tagging working points.

Table 5: Expected SM Event yields after the full event selection for three b-tagging working points Loose, Medium and Tight.

Process	WP=Loose	WP=Medium	WP=Tight
$t\bar{t}\gamma$+jet	1280	1401	1225
Wγ+jets	1465	329	86
Zγ+jets	315	232	92
Misidentifed photon	380	374	355
tγ(s-,tW-channel)	56	57	45
VVγ	36	8	5
Expected signal	167	154	115

DRAFT

5 Pileup re-weighting

A pileup re-weighting is applied to MC simulated samples to match the actual number of pile-up events distribution observed in the data. The minimum bias cross-section of 69.2 mb is used to calculate the true pileup distribution in data. The distributions of number of primary vertices after all selection criteria and before(up), after(down) pileup reweighting in data and simulation are shown in Figure 6.

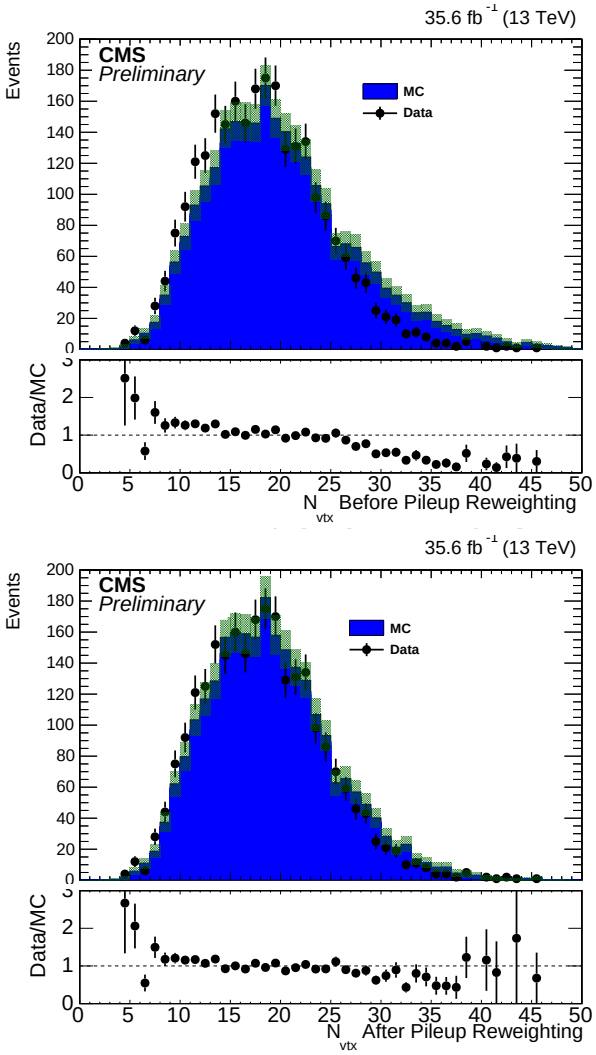

Figure 6: Distributions of the number of reconstructed vertices for signal events in data (black dots) and MC before(up) and after(down) applying the pileup reweighting.

6 Fake background estimation

As we already mentioned, all processes yielding one lepton, one photon, two or more jets, and missing transverse energy are possible sources of background. Generally reconstructed photon in the final state has a probability to be not real. Either electrons/positrons or Jets can be mis-reconstructed as photon.

Electrons due to small inefficiency of the tracker could be mis-reconstructed as photon. The contribution of such events become more significant if we consider the electron decay of the top quark. However, in our final state the main contribution of those events come from $t\bar{t}$ dileptonic decay channel when one of top/antitop quark decays into the muon and another top/antitop quark decays into the electron via decay of W boson. The amount of this background is estimated using the MC truth information by matching the reconstructed photon into the generator level object when generator object is either electron or positron.

Neutral hadrons (mostly $\pi^{0\prime}s$) originating from jet products can be misidentified as photons so-called "fake photons" with a very small possibility. However, the large cross section of these processes can result in significant jets fake photon contribution. Such signatures could come up when in the jet fragmentation, neutral pions appear and decay into two photons with a large boost. As a result, the two photon showers will overlap in the electromagnetic calorimeter and will not be separately distinguishable and they appear as a single photon in the detector. The ability for rejecting jets faking photons is crucial to suppress the QCD multijet background which has several orders of magnitude larger cross section with respect to the other background processes.

Processes such as W+jets, top quark pair, diboson, DY+jets, and single top quark with one jet fakes a photon would be a source of background. To find the contribution of these backgrounds, a data-driven approach called "ratio method" is used.

Estimation of the events containing a fake photon is made by defining a control region in data, enriched by such events. This enriched region is called "Photon-Like Jet (PLJ) sample" with the proper extrapolation factor to determine the fake normalization in the signal region [23].

6.1 Photon-like jet samples

In order to prepare the PLJ sample we keep all the analysis criteria for the other objects the same as before except the photon identification and isolation cuts. The photon selection items are those introduced in the official cut-based photon ID but they are re-designed in a way that mimic the jet but still being photon-like. To do that the photon isolation cuts are loosen

- pile-up corrected PF charged hadron isolation $PFCHIso < 10$
- pile-up corrected PF neutral hadron isolation $PFNIso < min(0.2 \times p_T^\gamma, 5 \times (10.91 + 0.0148431 p_T^\gamma + 0.000017 (p_T^\gamma)^2))$
- pile-up corrected PF photon isolation $PFIso < min(0.2 \times (p_T^\gamma)^2, 5 \times (3.63 + 0.0047 p_T^\gamma)$
- H/E < 0.0597
- Conversion safe electron veto

Afterwards events are required to satisfy at least on of the following criteria:

- shower shape $\sigma_{i\eta i\eta} > 0.0103$
- PF charged isolation > 1.295

It should be mentioned that the cut values for the H/E, $\sigma_{i\eta i\eta}$ and $PFChIso$ are those recommended by the Loose photon Id.

6.2 Fake photon fraction and extrapolation factor

To obtain the shape and normalization of fake backgrounds at first one needs to obtain the fake photon fraction (FPF) in the signal region. The FPF is defined as the ratio of the number of events with a fake photon to the total events, both in the signal region.

DRAFT

In practise using the FPF may enter a bias in the analysis as it is using the signal region information. Therefore to avoid any possible bias, we are not using the FPF for fake estimation but instead we transform this fake photon fraction into the extrapolation factor (EF). This EF is used to apply on the photon-like jet sample which is a suitable control region enriched by fake photons.

Using the EF, one can independently estimate the shape and normalization of the fake background in the signal region (without using any information of SR) by weighting each event in the photon-like jet sample to the amount of the EF. This is the way we estimate the contribution of events with the fake photons. In general, the fake photon fraction and extrapolation factor depends on photon p_T. Thus, in order to obtain a realistic modelling of this background we calculate FPFs and subsequently EFs in the different p_T bins of photon. To estimate the fake photon fraction in the signal region from data, two discriminating variables of photon selection which are assumed to be uncorrelated are used:

- shower shape $\sigma_{i\eta i\eta}$,
- PF charged isolation,

In order to examine the amount of correlation between PFCHIso and $\sigma_{i\eta i\eta}$, the MC simulated samples are used. Figure 7 shows the 2D plot of PFIso and $\sigma_{i\eta i\eta}$ of the fake photons (left) and real photons (right). The left plot has been obtained from the fake photons of $t\bar{t}$ and W+jets simulated samples in which the fake photons are found by comparison with generator level information. The value of correlation is found to be 4%. The right plot is obtained from the signal sample in which the prompt photons are matched with the photons at generator level which are from the matrix element. The correlation for the real photons in the right plot is less than 1%. These small amount of correlations for both real and fake photons prove that these variables are reasonably uncorrelated and are suitable to be used in the ratio method.

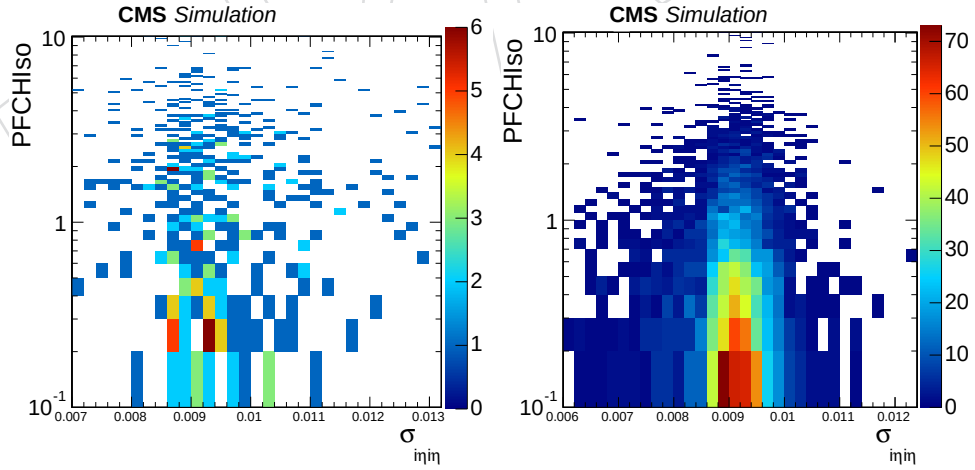

Figure 7: Two dimensional plot of the charged isolation and $\sigma_{i\eta i\eta}$ distribution for fake photons (left) and real photon (right). The plot for fake photons is obtained from the $t\bar{t}$and W+jets samples while the real photon plot in the right has been obtained using the signal sample.

Fig. 8, shows the two dimensional plot of $\sigma_{i\eta i\eta}$ and PFCHIso. Assuming a negligible correlation

between the two variables one has:

$$\frac{\text{Events with Fake photon in D}}{\text{Events in region C}} = \frac{\text{Events in region A}}{\text{Events in region B}}. \tag{7}$$

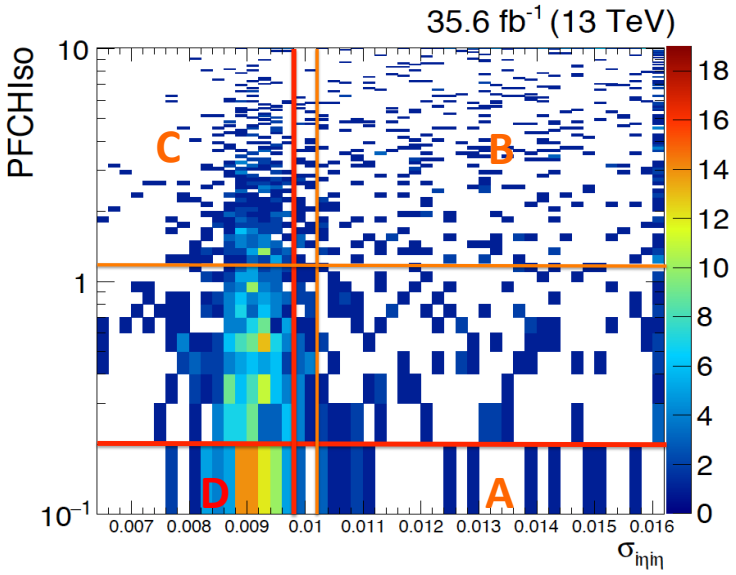

Figure 8: Two dimensional data histogram of the charged isolation and $\sigma_{i\eta i\eta}$ distribution, with photon transverse momentum larger than 25 GeV and $\eta < 1.4442$.

When all other criteria for photon selection are corresponding to the tight ID values, the region D is corresponding to the signal region while regions A, B, and C are sideband regions which are expected to be dominated by fake photons. Therefore, these sideband regions are defined by reversing at least one of the cut values for PFIso and $\sigma_{i\eta i\eta}$ (PFIso > 1.295 *or* $\sigma_{i\eta i\eta} > 0.01031$). The cut values used to construct the sideband regions for the PFCHIso and $\sigma_{i\eta i\eta}$ correspond to the values of Loose ID photon [15] which assure us the sideband regions are mainly dominated by the fake photons. Therefore, to obtain the fake photon fraction of events in the D region one could calculate as following:

$$\text{FPF}(p_T^\gamma) \text{ in region D} = \frac{\frac{\text{Events in region A} \times \text{Events in region C}}{\text{Events in region B}}}{\text{Total Events in region D}} \tag{8}$$

We have to mention that again here, In order to estimate the fake contribution we are not using the FPF as it was explained and discussed above. Then one could transform the fake photon fraction into the extrapolation factor for the PLJ sample by

$$\text{Extrapolation Factor}(p_T^\gamma) = \frac{\frac{\text{Events in region A} \times \text{Events in region C}}{\text{Events in region B}}}{\text{Events in photon-like jet sample}} \tag{9}$$

Figures 9 and 10 show the fake photon fraction and extrapolation factor of PLJ obtained in the different p_T bins of photon. The numerical values also are shown in the table 6. It should be

mentioned that the uncertainties on the values are only statistical. We will study the systematic uncertainties in detail in the next sections.

Table 6: The fake photon fractions (FPFs) and extrapolation fators (EFs) in six bins of photon transverse momentum.

	$p_{T,\gamma} \in [25,35]$	$[35,45]$	$[45,65]$	$[65,85]$	$[85,125]$	$[125,\infty]$
FPF	0.21 ± 0.02	0.18 ± 0.03	0.13 ± 0.02	0.07 ± 0.02	0.08 ± 0.03	0.03 ± 0.01
EF	0.062 ± 0.006	0.066 ± 0.010	0.047 ± 0.008	0.031 ± 0.009	0.030 ± 0.010	0.016 ± 0.007

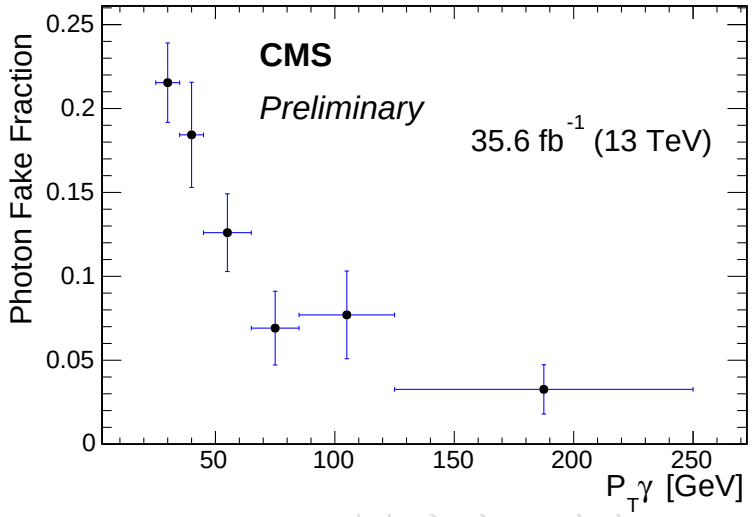

Figure 9: The fake photon fraction calculated from the ratio method in terms of photon transverse momentum.

6.3 Systematic uncertainties and closure test for fake estimation

There are several sources of uncertainty for estimation of events containing a fake photon. The first relevant source of uncertainty entering into the analysis from this method comes from the sideband region definition which affects directly the calculated fake photon fraction. This uncertainty in principle is due to the correlation between the isolation variable and the shower shape variable. Any correlation between PF charge isolation and $\sigma_{i\eta i\eta}$ leads to change in sideband region when one variable changes and leads to different values of fake photon fractions in photon p_T bins.

To consider the amount of this uncertainty, we change the border of sideband region in a way that we have two statistically equal samples. Then FPF is recalculated using both samples and take the half of their difference as the systematic uncertainty due to sideband region definition, which affects both normalization and shape of distributions. The amount of this uncertainty is increasing from 2% to 34% when one goes into the higher p_{T} bins of photon. The reason for that as it was expected and discussed above is known. When we move to higher p_{T} bins and calculate the correlation of these two variables in each p_{T} bin, the amount of correlation is also increasing and directly reflect on this uncertainty.

Additional source that has an impact on the fake photon fraction comes from possible contaminations of prompt photons in the regions A, B, and C. This is considered as a source of

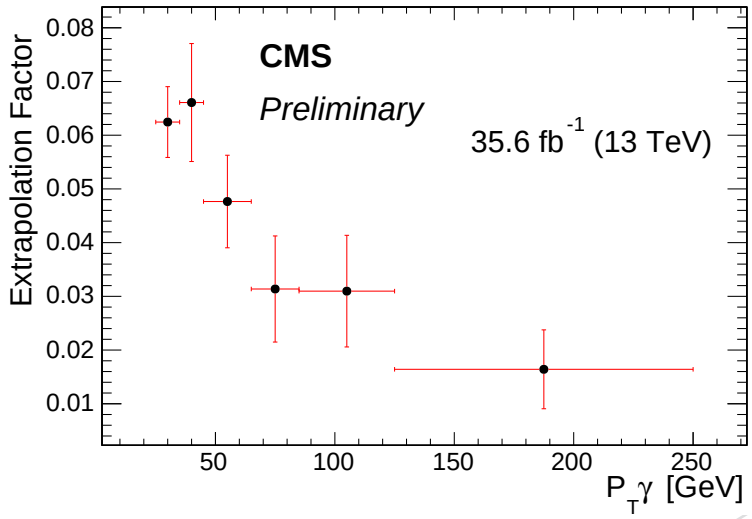

Figure 10: The extrapolation factor for PLJ sample calculated from the ratio method in terms of photon transverse momentum.

systematic uncertainty in calculation of the fake photon fraction. In fake photon fraction calculation in each photon p_{T} bin, the number of fake in the regions of A,B, and C are varied within the number of prompt photons and the change in the fake photon fraction and subsequently in the extrapolation factor for PLJ sample in each bin is calculated. This is taken as the source of systematic uncertainty due to the prompt photon contamination on the fake background estimation. We found the amount of this uncertainty is varying between $7-10\%$ depending on the photon p_{T} therefore, we consider a conservative value of 10%.

The statistical uncertainty is also considered as another source of uncertainty in the fake background estimation as the fake photon fraction in each photon transverse momentum bin has an uncertainty which increases with photon p_T.

The uncertainty on the fake estimation due to each mentioned sources and for each bin of photon p_{T} are shown in the Table 7 .

Table 7: Impact of each sources of uncertainty in the fake photon fraction

	$p_{T,\gamma} \in [25,35]$	$[35,45]$	$[45,65]$	$[65,85]$	$[85,125]$	$[125,\infty]$
Sideband region	2%	1%	13%	16%	20%	34%
Real photon	10%	10%	10%	10%	10%	10%
Statistical	10%	16%	15%	28%	37%	33%

In order to validate the method for fake estimation, we calculate the FPF using MC truth information. To do that we match all the photons at the reconstruction level with the generator level and categorized MC events from different processes into the fake and real photons. Then the FPF is calculated in each bin of photon p_T using the following formula:

$$\mathrm{FPF}(p_T^{\gamma}) \text{ in region D} = \frac{\text{Events with Fake photon in D (MC truth)}}{\text{Total Events in region D (MC)}} \tag{10}$$

The calculated FPF using the MC truth information shows good agreement with the one cal-

DRAFT

culated using ratio method which ensures us the compatibility of this method. The numerical values for FPF using the data(ratio method) and using the MC truth information are shown in the Table 8. In the first row the errors include the statistical and systematical uncertainties while for the second row errors are only statistical.

Table 8: The fake photon fractions using data (Ratio method) and MC truth information in six bins of photon transverse momentum.

	$p_{T,\gamma} \in [25,35]$	$[35,45]$	$[45,65]$	$[65,85]$	$[85,125]$	$[125,\infty]$
FPF (Data)	0.21 ± 0.03	0.18 ± 0.03	0.13 ± 0.03	0.07 ± 0.02	0.08 ± 0.03	0.03 ± 0.01
FPF (MC Truth)	0.22 ± 0.02	0.19 ± 0.02	0.16 ± 0.02	0.11 ± 0.02	0.11 ± 0.03	0.05 ± 0.01

7 $t\bar{t}\gamma$+jets background estimation

$t\bar{t}+\gamma$+jet is the main background process which contributes into our final state. Furthermore, for estimation of this background from simulation one has to have large enough statistics and take into account several theoretical sources of systematic uncertainties such as scales variation and showering etc. As a result, in this analysis this background is predicted using data. In order to study this background independently from MC simulation we are defining a control region using the data which is enriched by this process as following:

(i) the region with exactly two b-tagged jets,
(ii) all other selection criteria the same as in the signal region.

In the defined control region the purity of $t\bar{t}+\gamma$+jet found to be 84%. However, in order to have a quite pure $t\bar{t}+\gamma$+jet control region, we subtract the contribution of all the rest background processes from data i.e., the fake and other backgrounds like W+γ+jet, Z+γ+jet, diboson and single top s- and tW-channels.

In this $t\bar{t}+\gamma$+jet control region, among all the rest background processes, the dominant one comes from the events with fake photons. It is notable that in order to estimate the fake photon events, we use the same data-driven method as explained previously but for this control region. Contribution of signal in this CR is 2% which is very low and could be neglected.

Comparing the estimated $t\bar{t}+\gamma$+jet from data and from MC simulation, we found the ratio of events in data to the one in simulation equal to 1.07 ± 0.06, where the uncertainty is only statistical.

To make sure that the defined control region for the $t\bar{t} + \gamma$+jet is estimated well and is in reasonable agreement with data, some control region plots are presented in Figures 11, 12, 13.

The strategy to estimate this background is to obtain the shape of this process from the defined control region while the normalization left as a float number in the final fit on the MVA output. One can extract the normalization of $t\bar{t}+\gamma$+jet process as well as the signal cross section simultaneously by fitting into the data in the signal region as well as control region which is going to be discussed in details in the section 11. The systematic uncertainty on the $t\bar{t}+\gamma$+jet estimation consists of a statistical uncertainty and also the amount of uncertainties from the fake and the rest simulation-based backgrounds in the $t\bar{t}+\gamma$+jet control region.

DRAFT

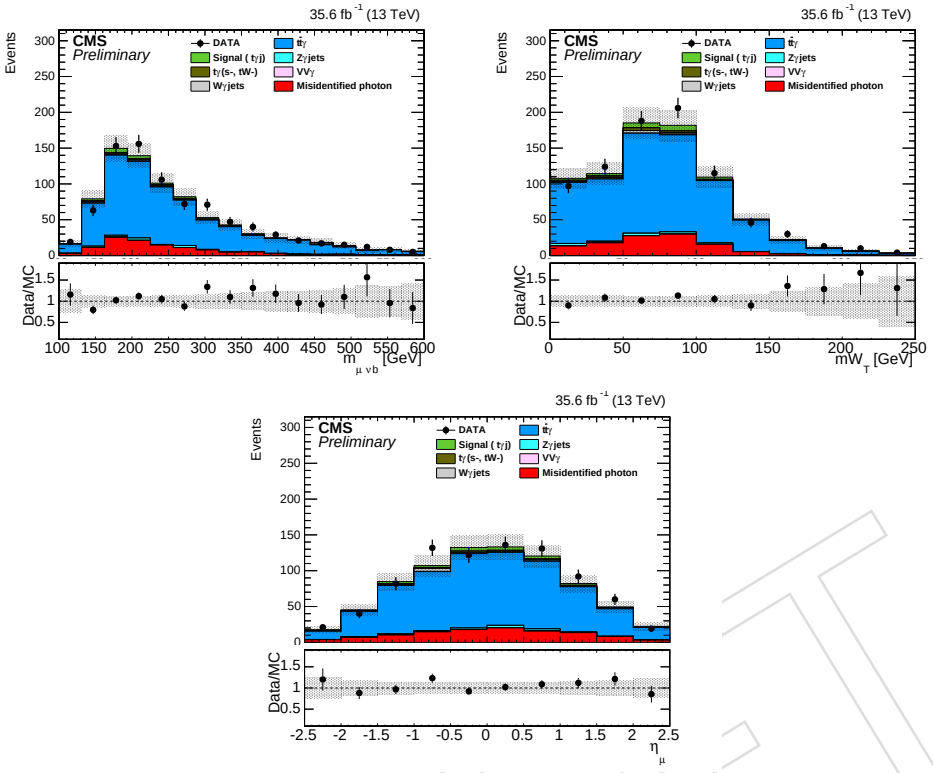

Figure 11: The distributions of top mass, transverse mass of W boson, η of muon. Error bands indicate both statistical and systematical uncertainties.

8 Signal and background discrimination

The SM prediction for signal is much smaller than the background processes, consequently it is important to increase the separation between signal and background events to be able to measure the single top plus a photon cross section with highest possible significance. A multivariate classification approach, Boosted Decision Tree (BDT), is chosen to optimize the discrimination between SM and possible signal events.

The following eight variables are chosen to construct a BDT according to their separation power:

- Pseudorapidity of the light jet,
- Cosine angle of muon and light-jet in the top rest frame,
- Pseudorapidity of the Muon candidate,
- Angular separation of the light-jet and photon $\Delta R(l - jet, \gamma)$,
- Reconstructed top quark mass m_{top},
- Jet multiplicity,
- Reconstructed transverse mass of W boson,
- Charge of muon candidate

Table 9 shows some parameters which is used for the BDT training.

DRAFT

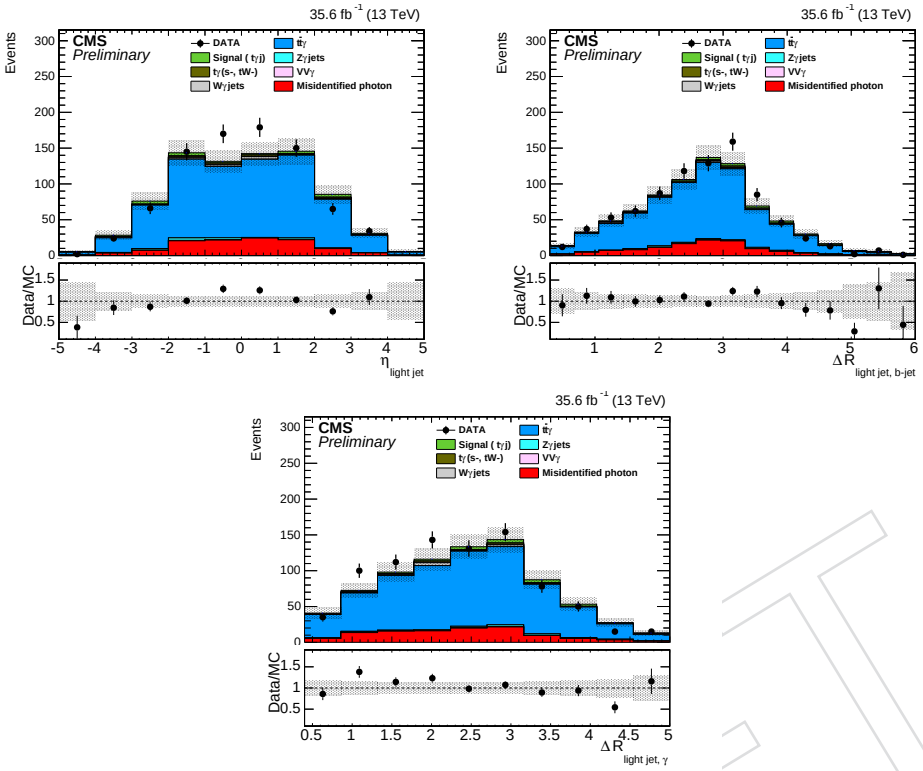

Figure 12: The distributions of η of light jet, $\Delta R(\text{-}jet, light-jet)$, $\Delta R(\gamma, light-jet)$. Error bands indicate both statistical and systematical uncertainties.

Table 9: BDT parameters used for training

parameter	Value
NTrees	850
BoostType	AdaBoost
nCuts	20
MaxDepth	3

The BDT needs to be trained to obtain a good separation of signal from the background. To do so, the $t\bar{t}$+γ+jet background sample is used to train the BDT against the signal.

Figure 14 shows the normalized distributions of all BDT input variables after training for signal and for the $t\bar{t}$+γ+jet background. The blue distributions indicate the signal distributions and the red dashed distributions present the background shapes. As it can be seen, these set of variables discriminate signal from background significantly. Figure 15 depicts the two-dimensional plot which shows the linear correlation of the input variables to BDT for signal and for the background.

In Fig. 16 we compare the BDT output from the training and the testing samples. As it can be seen no strange behaviour is observed and the effects of overtraining can be safely neglected.

The BDT output of signal and background is very well separated which confirms the power of the BDT input variables to discriminate signal from background. Finally, the plot of background rejection versus signal efficiency is presented in Fig. 17.

DRAFT

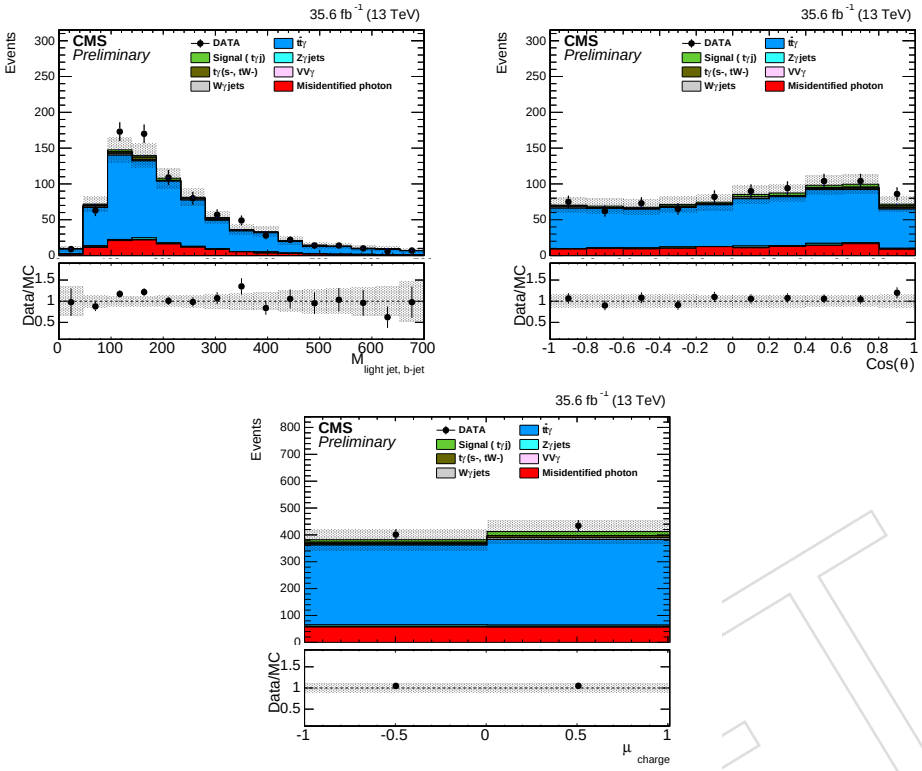

Figure 13: The distributions of invariant mass of light jet and b-jet , cosine of muon and light-jet in the top rest frame and charge of muon. Error bands indicate both statistical and systematical uncertainties.

To make sure that the extracted shape of main background i.e. $t\bar{t}$+γ+jets from control region has the same behaviour as signal region, the BDT output variable (x_{BDT}) is compared in these two regions. Fig. 18 shows the distribution of x_{BDT} for $t\bar{t}$+γ+jets in signal region and control region. It should be mentioned that the both x_{BDT} shapes in control region and the signal region are extracted from simulation. In order to account the possible difference in the x_{BDT} shape from SR and CR, we consider a source of systematic error on the shape of $t\bar{t} + \gamma + jet$ due to this difference in the measurement procedure.

9 W+γ+jets background cross check

W+γ+jets is one of the background process which has a contribution in the $t + \gamma$ final state. However, due to requirement of one exactly medium b-tagged jet the contribution of this process in the final state is not large. Therefore, in this analysis W+γ+jets process is estimated using the MC simulated samples. Regardless of how important this background is in the final state, one can examine the shape and normalization produced by the simulation with the control region for this process which is defined as following:

(i) require to have zero b-tagged jets,
(ii) all other selection criteria the same as in the signal region.

DRAFT

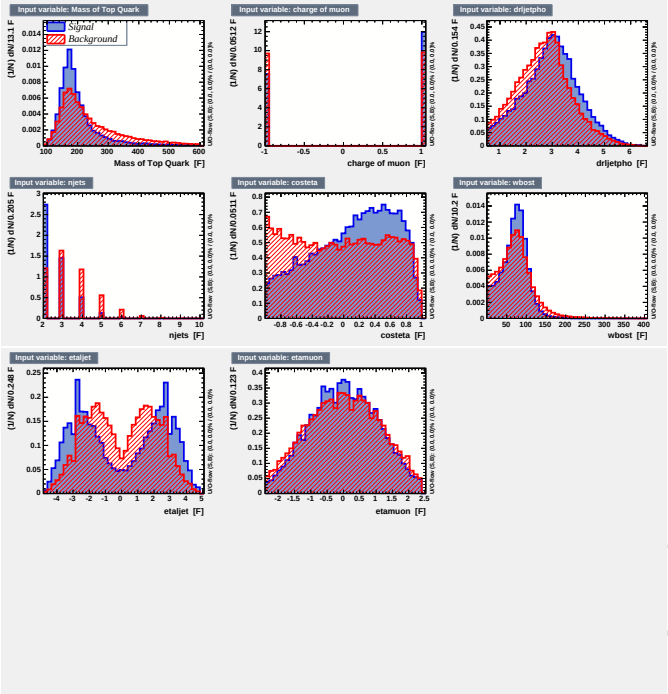

Figure 14: The distributions of the BDT input variables for signal and $t\bar{t}$ + γ+jet after training, blue is the signal and red is for the background.

The purity of this control region is 88% while the contribution of signal is about 1.5% which is negligible. In order to cross check weather the BDT shape of this process is well produced one can compare the BDT output shape in the signal region using the MC with the BDT shape in the control region using the data. Therefore to obtain the shape of BDT in the CR using the data one has to subtract the contribution of rest backgrounds using simulation. Figure 19 shows the comparison between the BDT shape of W+γ+jets process in the signal region(using the MC) with the control region (using the data) which shows very good agreement and convinced us to rely on the simulation. It should be mentioned that the error are only statistical for both signal region and control region distributions.

10 Systematic uncertainties

The source and impact of systematics uncertainties are discussed in this section. In this section we categorize the systematic uncertainties depending on the procedure we use for estimation of that process.

Contribution of events with a fake photon is estimated using the ratio method and relevant systematic sources which was discussed in the section 6.3 and listed in the table 7 are applied for this background which affects both the shape and normalization of this background.

$t\bar{t}$+γ+jet process which is the dominant background of this analysis is estimated by defining a CR which was explained in the section 9. The systematic uncertainty on estimation of $t\bar{t}$+γ+jet has been discussed in the section 9.

Other processes like W+γ+jet, Z+γ+jet, diboson and single top s- and tW-channels are esti-

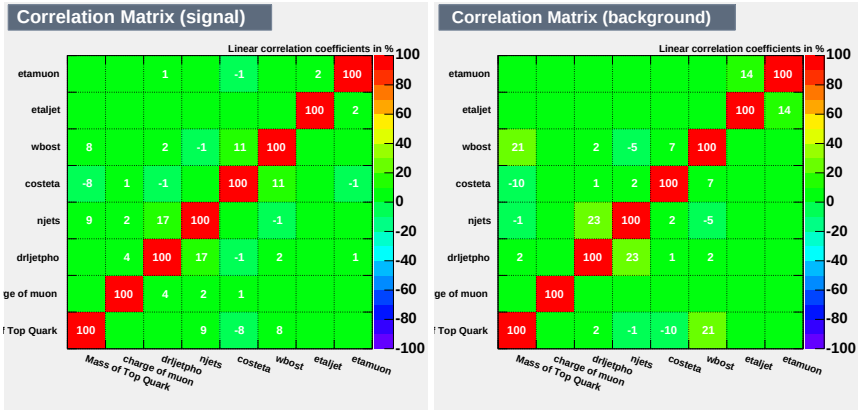

Figure 15: The correlation matrices for signal (left) and for background.

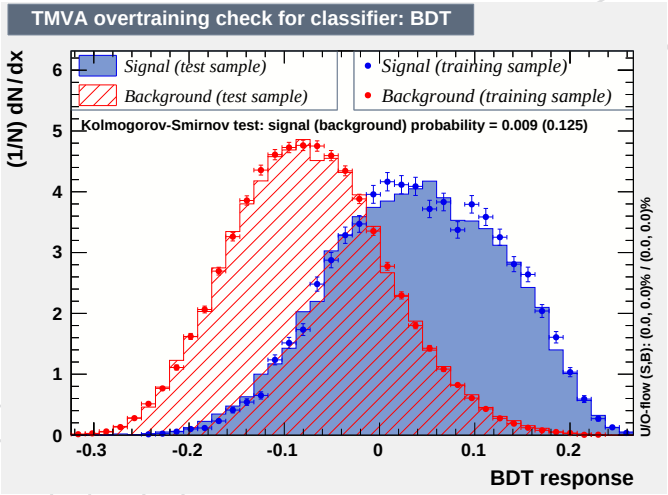

Figure 16: The BDT output distribution for overtraining check.

mated using the MC simulated samples and following source of uncertainties listed below are considered for those processes.

- *Pile-up* : To estimate the pileup uncertainty, the minimum bias cross section is shifted up and down by 4.6%. This source is treated as a normalization uncertainty in the fit.
- *Jet energy corrections (JES and JER)*: The recent recommendation for jet energy resolution measurements is used in this analysis [24]. Each jet in MC samples is smeared up/down depending on its transverse momentum (p_T) and pseudorapidity (η) with respect to the central value measured in data. As for jet energy scale, a parameterization dependent on p_T and η of jet is used to vary the calibration of the jets in the simulation. The parameterization has been prepared by the JetMET POG. When varying the jet energy scale, the missing transverse energy $E_{\mathrm{T,miss}}$ estimate is updated.

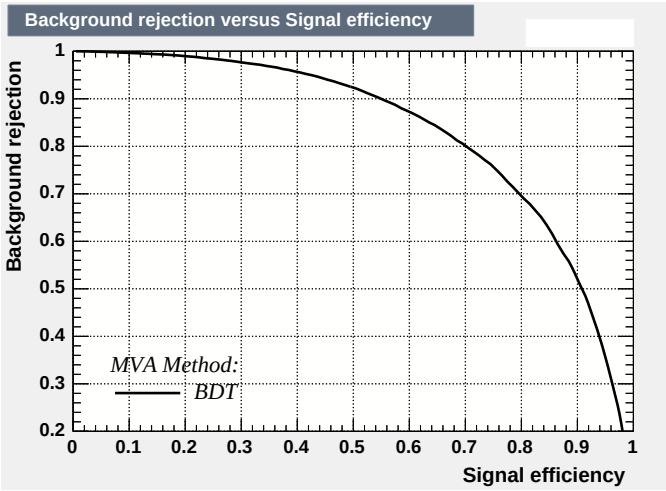

Figure 17: The ROC curve for background rejection versus signal efficiency.

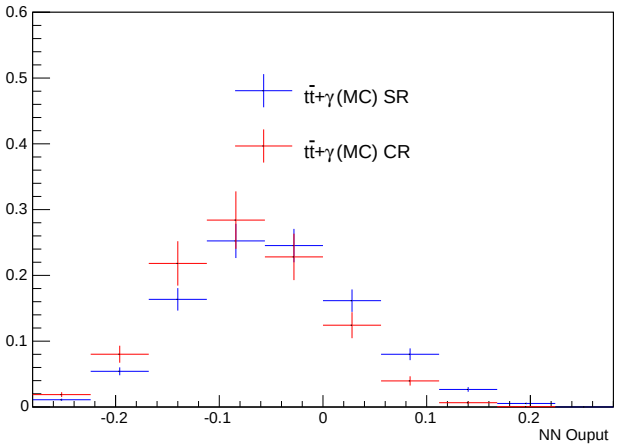

Figure 18: The distributions of x_{BDT} in signal region and control region for $t\bar{t}+\gamma$+jets events.

- *Photon reconstruction and identification*: The photon reconstruction, and identification efficiencies are applied. The uncertainties in the scale factors, which are used to correct the simulation to match the data are considered [25].
- *Photon Energy Scale*: In order to estimate the photon energy scale, the photon energy is varied by 1% in barrel [25].
- *Lepton reconstruction, identification, and isolation* :The lepton reconstruction, and identification efficiencies are evaluated with tag-and-probe techniques using Z boson dilepton decays. The uncertainties in the scale factors, which are used to correct the simulation to match the data, take into account the different lepton selection efficiencies in different Runs.
- *Background normalization*: Normalization uncertainties of $t\bar{t}$[26], $t\bar{t}+\gamma$ [27], $W\gamma$+jet

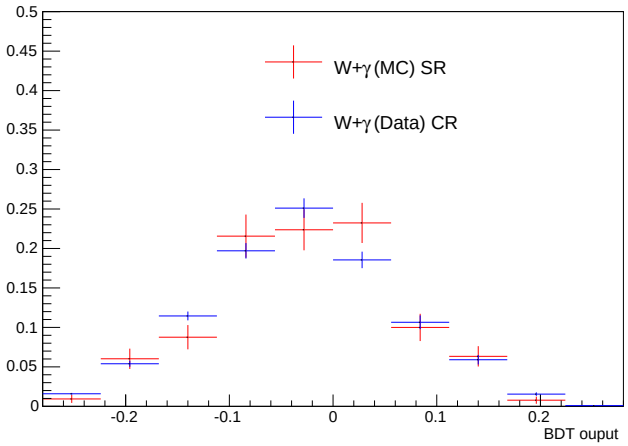

Figure 19: Comparison of BDT shape of W+γ+jets process in the signal region(using the MC) with the control region (using the data). Errors are only statistical

[23], Zγ+jets [28], diboson [29], single top t-channel [30] are 4%, 21%, 20%, 26%, 8%, 13%, respectively, which are assigned to each background source separately. The uncertainty on the normalizations of single top quark productions in s- and tW-channels are taken to be 4% and 5.5% Ref.[31], respectively. This is applied for the backgrounds which have been obtained from simulation.

- *Trigger*: The uncertainty on the trigger data-to-MC scale factors as a function of p_T and η is applied.
- *b tagging and mis-tagging*: To account for the efficiency difference in b-tagging and misidentification between data and Monte Carlo simulation, b-tagging POG scale factors are applied to each jet as a function of jet p_T and η [32]. The systematic effect is estimated by shifting up and down $\pm 1\sigma$ of the scale factor as a shape nuisance in the fit.
- *Integrated luminosity*: Integrated luminosity is estimated from data, and amounts to a 2.5% uncertainty on the signal yield [7].
- *Unclustered particles*: The uncertainty due to unclustered particles considered by varying energy of each particle according to the detector measured resolutions as it is recommended by JetMET POG [33].
- *Electron Veto Id*: The uncertainty due to the implemented scale factor of electron veto Id based on the recommendation of EGamma POG is applied[25].

In addition to the above items, the following sources of the systematic uncertainties are applied on the signal sample:

- *Parton density functions (PDF) uncertainties*: The effect of the uncertainty from the choice of PDF is assessed by estimating the relative yield variation in each bin of the observable variables and category, after re-weighting the events of the simulated signal sample.
- *The renormalization and factorization scales uncertainty:* The uncertainty from the choice of factorization and renormalization scales in the QCD calculations is based

DRAFT

on dedicated simulated samples signal production with the scales varied from half to twice their nominal values.

- *Hadronization/Showering*: The uncertainty due to the showering and hadronization model is determined by comparing samples simulated with MADGRAPH5_AMC@NLO using either PYTHIA or HERWIG [34] for showering and hadronization.

Among the above uncertainties, the luminosity uncertainty and background normalization uncertainty affect the normalization but we also consider trigger, photon energy scale, lepton selection, reconstruction efficiencies, unclustered particles and jet energy resolution on the normalization as they are very small while, the uncertainties from the photon selection efficiencies, b tagging, jet energy scale, and pileup affect both BDT shape and normalization for signal and background. The uncertainties due to PDF, variation of renormalization and factorization scales and Hadronization/Showering are only applied to the signal. Table 10 shows applied systematic uncertainties for each process in the measurement procedure. It also shows whether each process is affected by shape or normalization.

Table 10: Applied uncertainties for each process and the way that each process is affected by relevant uncertainties are presented.

Process	W+γ+jet		Z+γ+jet		Diboson		tw-ch,s-ch		$t\bar{t}$+γ+jet		Misidentified		Signal	
	shape	norm	shape	norm	shape	norm	shape	norm	shape	norm	shape	norm	shape	norm
Luminosity	×	✓	×	✓	×	✓	×	✓	×	×	×	×	×	✓
Lep rec/id	×	✓	×	✓	×	✓	×	✓	×	×	×	×	×	✓
Photon ES	×	✓	×	✓	×	✓	×	✓	×	×	×	×	×	✓
Photon Id	✓	✓	✓	✓	✓	✓	✓	✓	×	×	×	×	✓	✓
Trigger	×	✓	×	✓	×	✓	×	✓	×	×	×	×	×	✓
PDF	×	×	×	×	×	×	×	×	×	×	×	×	✓	✓
Q-scale	×	×	×	×	×	×	×	×	×	×	×	×	✓	✓
Pileup	✓	✓	✓	✓	✓	✓	✓	✓	×	×	×	×	✓	✓
Fake	×	×	×	×	×	×	×	×	×	×	✓	✓	×	×
Back norm	×	✓	×	✓	×	✓	×	✓	×	×	×	×	×	×
JES	✓	✓	✓	✓	✓	✓	✓	✓	×	×	×	×	✓	✓
JER	×	✓	×	✓	×	✓	×	✓	×	×	×	×	×	✓
Signal Model	×	×	×	×	×	×	×	×	×	×	×	×	✓	✓
b-tagging	✓	✓	✓	✓	✓	✓	✓	✓	×	×	×	×	✓	✓
Uncl part	×	✓	×	✓	×	✓	×	✓	×	×	×	×	×	✓
$t\bar{t}\gamma$ CR	×	×	×	×	×	×	×	×	×	✓	×	×	×	×
$t\bar{t}\gamma$ CR shape	×	×	×	×	×	×	×	×	✓	✓	×	×	×	×
EleVeto SF	✓	✓	✓	✓	✓	✓	✓	✓	×	×	×	×	✓	✓

11 Cross section measurement and significance calculation

We perform a simultaneous binned likelihood fit to the rate and shape of the BDT distribution x_{BDT} after all selection criteria. The signal region BDT output x_{BDT} in data is parameterized as:

$$F(x_{BDT}) = C_{signal}S_{signal}(x_{BDT}) + C_{W\gamma jet}S_{W\gamma jet}(x_{BDT}) + C_{t\bar{t}\gamma jet}S_{t\bar{t}\gamma jet}(x_{BDT}) + C_{Z\gamma jet}S_{Z\gamma jet}(x_{BDT}) + C_{fake}S_{fake}(x_{BDT}) + C_{B}S_{B}(x_{BDT}), \quad (11)$$

where $S_{signal}(x_{BDT})$, $S_{W\gamma jet}(x_{BDT})$, $S_{t\bar{t}\gamma jet}(x_{BDT})$, $S_{Z\gamma jet}(x_{BDT})$, $S_{fake}(x_{BDT})$ and $S_{B}(x_{BDT})$ are, respectively, the templates for signal, W+γ+jets, $t\bar{t}$+γ+jet, Zγ+jets, fake events and the sum of all

other backgrounds. C_{signal}, $C_{W\gamma jet}$, $C_{t\bar{t}\gamma jet}$, $C_{Z\gamma jet}$, $C_{fake}$and C_B are the corresponding normalizations for each distribution from which C_{signal} and $C_{t\bar{t}+\gamma jet}$ are unknown and extracted from the fit. Both the normalization and the distribution of the misidentified photon background, i.e., the C_{fake} and $S_{fake}(x_{BDT})$ are obtained from data based on the ratio method. The normalization and the distribution of sum of all other backgrounds are derived from simulation. The distribution for signal ($S_{signal}(x_{BDT})$) is taken from simulation and for $t\bar{t}$+γ+jet ($S_{t\bar{t}\gamma jet}(x_{BDT})$) from data in a control region defined by requiring exactly two b-tagged jets.

In the likelihood function, to each source of systematic uncertainty u, a nuisance parameter θ_u is dedicated. The production rates of signal and backgrounds are allowed to vary in the fit within the systematic uncertainties. The sensitivity to signal is estimated using the derivative of the likelihood test statistic, defined as:

$$q = \frac{\partial}{\partial\mu} ln\mathcal{L}(\mu = 0, \hat{\theta}_0|data), \tag{12}$$

where the signal strength parameter is denoted by μ and $\hat{\theta}_0$ is the set of nuisance parameters. In order to construct the distribution of the test statistic for the background-only and signal + background hypotheses, pseudo-data are generated. The nuisance parameters are allowed to vary according to their prior distributions in the pseudo-experiments. In q evaluation, the likelihood is maximized only w.r.t the normalizations of background and nuisance parameters. To perform the calculations, HiggsAnalysis-CombinedLimit tool [35] is used. A profile likelihood method is utilized to determine the production cross section of the signal and 68% confidence level interval.

Figure 20 shows the impact of systematic uncertainties for the likelihood fit. This impact evaluated by fixing the rest of systematics and let only one of them change in the fit procedure.

In Table 10, the impact of systematic uncertainties on measured cross section due to each source in presented. The impact for each nuisance parameter is obtained from the shift on the measured signal cross section which is induced by changing that particular nuisance parameter into the 1σ and -1σ of it's post-fit values while the rest are profiled normally.

A total of 2535 events are selected in data and, $2402^{+180}_{-177}(Stat + Syst)$ background events are expected, where the both statistical and systematical uncertainties are mentioned. The expected amount of SM background is dominated by the $t\bar{t}$+γ+jets process, amounting to 1401^{+131}_{-131}. The contributions of W+γ+jet and Z+γ+jets are found to be 329^{+79}_{-77} and 232^{+59}_{-52}, respectively. The fake background contribution has been estimated based on the method described in Sec.6 and is 374^{+74}_{-74}. Single top quark (s-, and tW-channel) and VVγ contributions are 57^{+8}_{-9} and 8^{+3}_{-3}, respectively. The expected number of signal events is 154^{+24}_{-24}.

The number of events for data and for each source of background after full selection is presented in Table 12. The uncertainties on the expected yields include both statistical and systematic.

An excess of events above the expected background events with a p-value of 4.27×10^{-6} which corresponds to a significance of 4.4σ is obtained. It should be mentioned that the only background normalization which is not given into the fit and it is expected to extract from the final fit to the data is belong to $t\bar{t}$+γ+jets which is found to be 1221 ± 121. The expected significance from simulation is found to be 3.0σ. The measured cross section of $\sigma(t\gamma)\mathcal{B}$ in the region $E_{T,\gamma} > 25$ GeV, $|\eta| < 1.444$,and $\Delta R(X, \gamma) > 0.5$, where $X = \mu$,b-jet,light-jet, is found to be $115 \pm ^{+37}_{-32}$(stat $\oplus$ syst) fb which is in agreement with the SM predicted value of 81 fb.

DRAFT

Table 11: Impact of each source of systematic uncertainty to the signal cross section measurement is obtained from the shift on the measured signal cross section which is induced by changing that particular nuisance parameter into the 1σ and -1σ of it's post-fit values while the rest are profiled normally.

Source	Uncertainty %
JES and JER	12%
b tagging and mistag efficiency	7%
Integrated luminosity	5%
Pileup	5%
Fake background	4%
Photon identification and isolation	3%
Photon energy scale	1%
MET	1%
Signal modelling	9%
Renormalization and factorization scales	6%
PDF	5%
$Z\gamma$+jets cross section	8%
$t\bar{t}+\gamma$ cross section	4%
$W\gamma$+jets cross section	3%
$t\bar{t}+\gamma$ shape	5%
Statistical	15%

DRAFT

Table 12: Event yields after the full event selection in data and each source of SM background contribution. The expected yields are presented with both statistical and systematical uncertainties.

Process	Event yield $\pm$ (stat $\oplus$ syst)
$t\bar{t}\gamma$+jet	1401^{+131}_{-131}
$W\gamma$+jets	329^{+79}_{-77}
$Z\gamma$+jets	232^{+59}_{-52}
Misidentifed photon	374^{+74}_{-74}
$t\gamma$(s-,tW-channel)	57^{+8}_{-9}
$VV\gamma$	8^{+3}_{-3}
Total background	2402^{+180}_{-177}
Expected signal	154^{+24}_{-24}
Data	2535

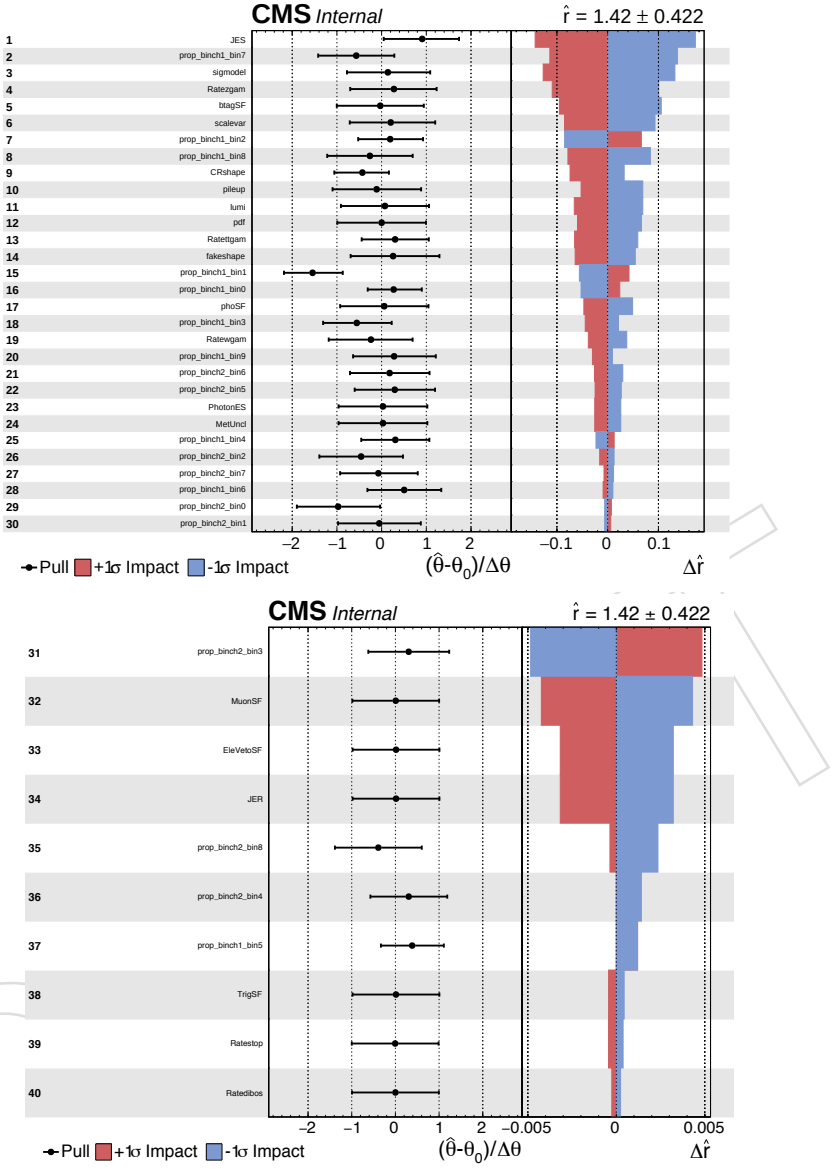

Figure 20: Observed impact of systematic uncertainties on the signal strength

To assess the quality of the modelling provided by the MC simulation and data-driven background estimations, we make comparisons between data and the SM prediction which normalized to the luminosity after all selection criteria. Figures 21 and 22 show the transverse momenta and pseudorapidity distributions of the muon, photon, b-jet, and light jet. The distributions of missing transverse energy, Invariant mass of light-jet and b-jet, angular separations between light-jet and photon, and light-jet and b-jet and cosine angle of muon and light-jet in the top quark rest frame are presented in Fig.23. As it can be seen, we find a good agreement for all the basic kinematic observables. The reconstructed top quark mass, invariant mass of the top quark and the photon candidate, and $\Delta R(top, \gamma)$ distributions are presented in Fig.25. The top quark is reconstructed based on the method explained in Sec.4.3.

The BDT distribution before and after the fit are depicted in Fig.26 and 27.

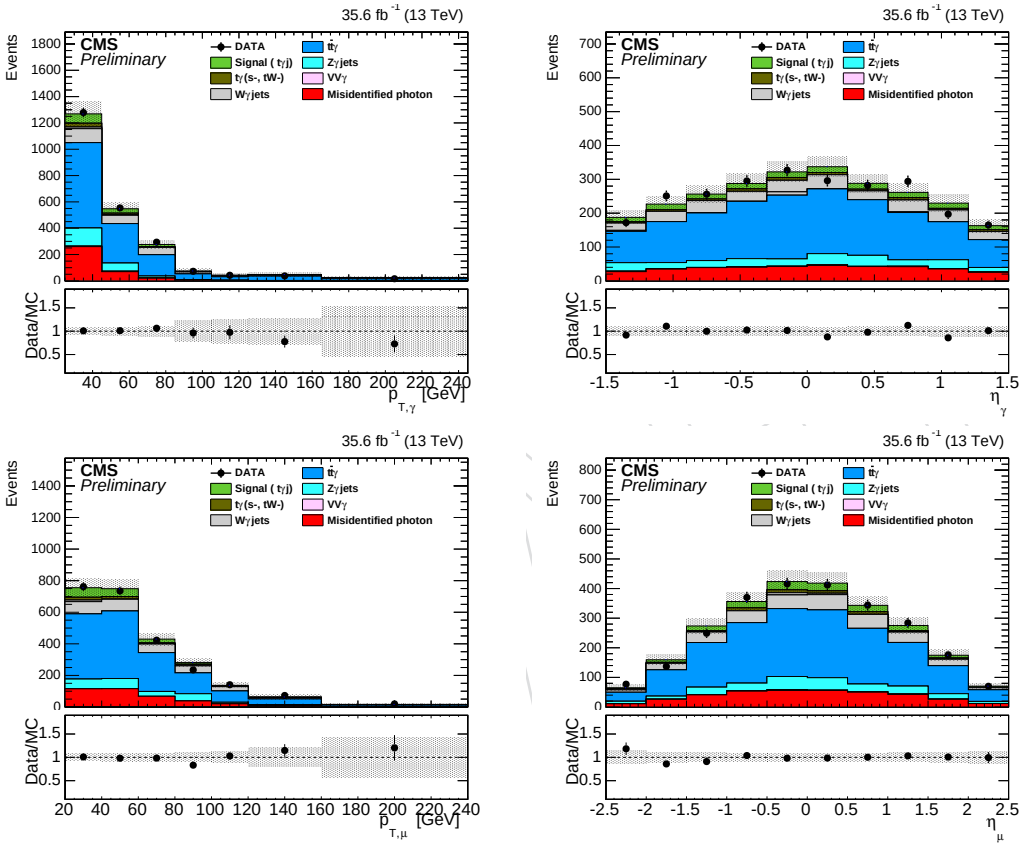

Figure 21: Distributions of p_T and η of the photon (top), the p_T and η of the muon (bottom) after the final event selection and background estimations. The uncertainty band includes both statistical and systematical ones.

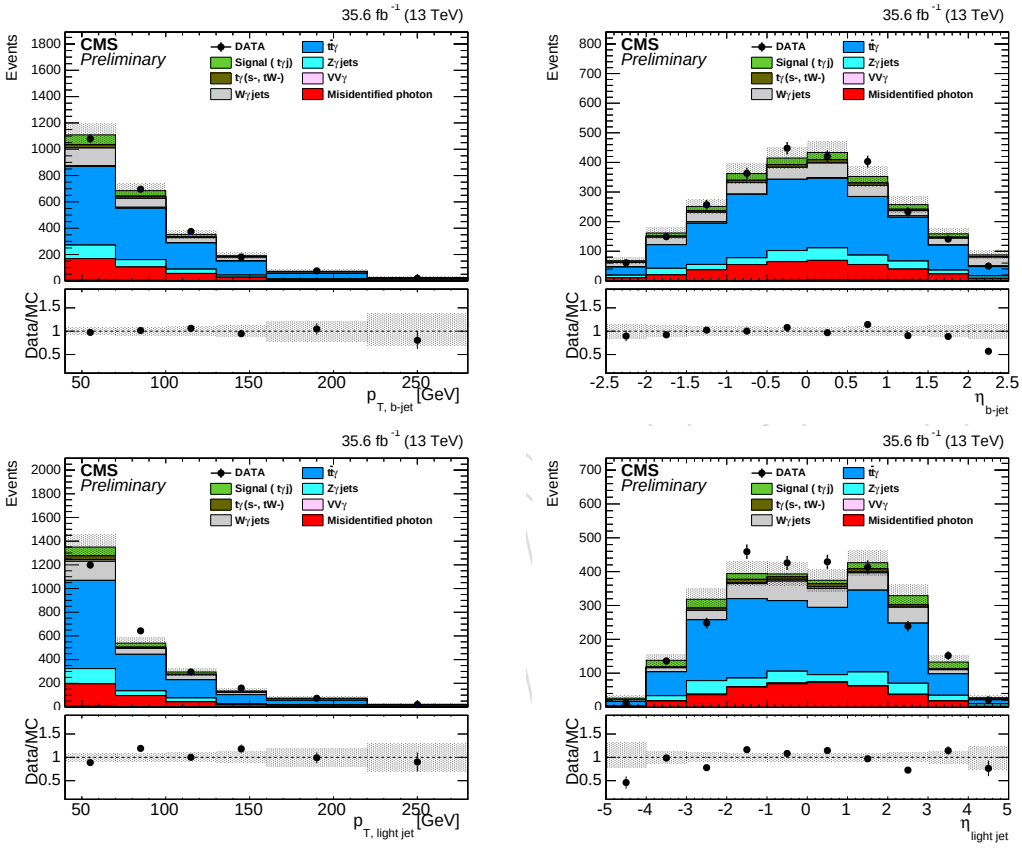

Figure 22: Distributions of p_T and η of the b-jet (top), the p_T and η of the light jet (bottom) after the final event selection and background estimations. The uncertainty band includes both statistical and systematical ones.

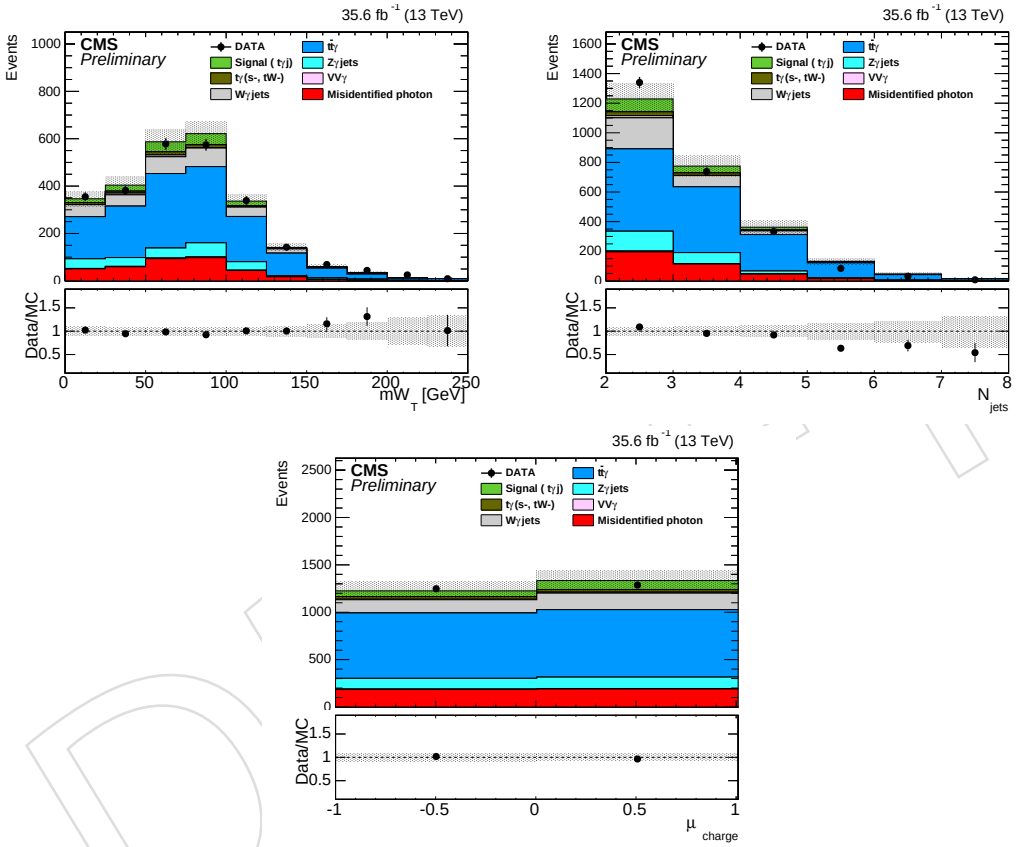

Figure 23: Distributions of transverse mass of W boson, number of total jets and charge of muon after the final event selection and background estimations. The uncertainty band includes the statistical and systematics ones.

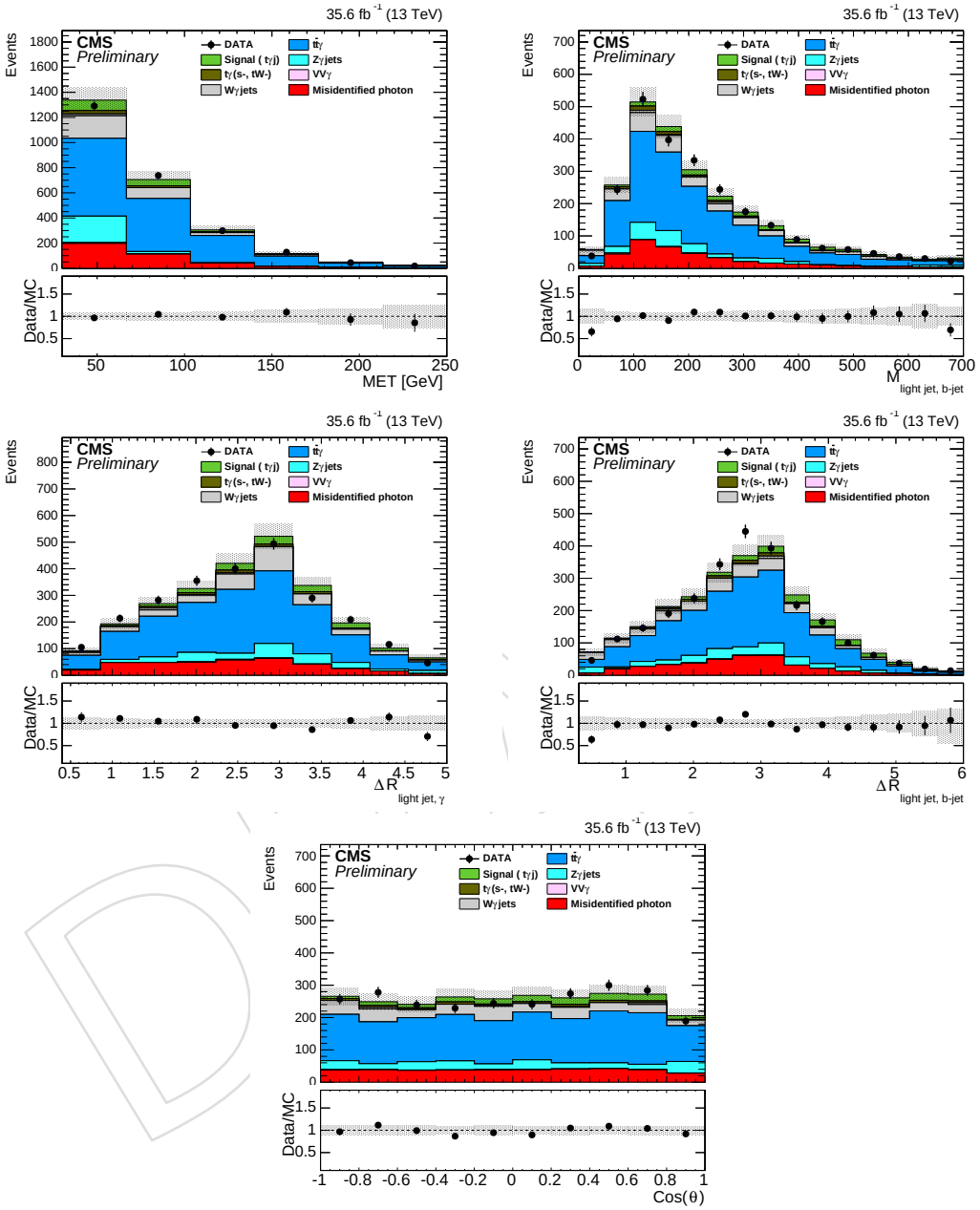

Figure 24: Distributions of missing transverse energy MET, invariant mass of b and light-jet, the $\Delta R(light-jet,\gamma)$ and $\Delta R(light-jet,bjet-jet)$ (middle), charge of the muon (bottom) after the final event selection and background estimations. The uncertainty band includes both statistical and systematical ones.

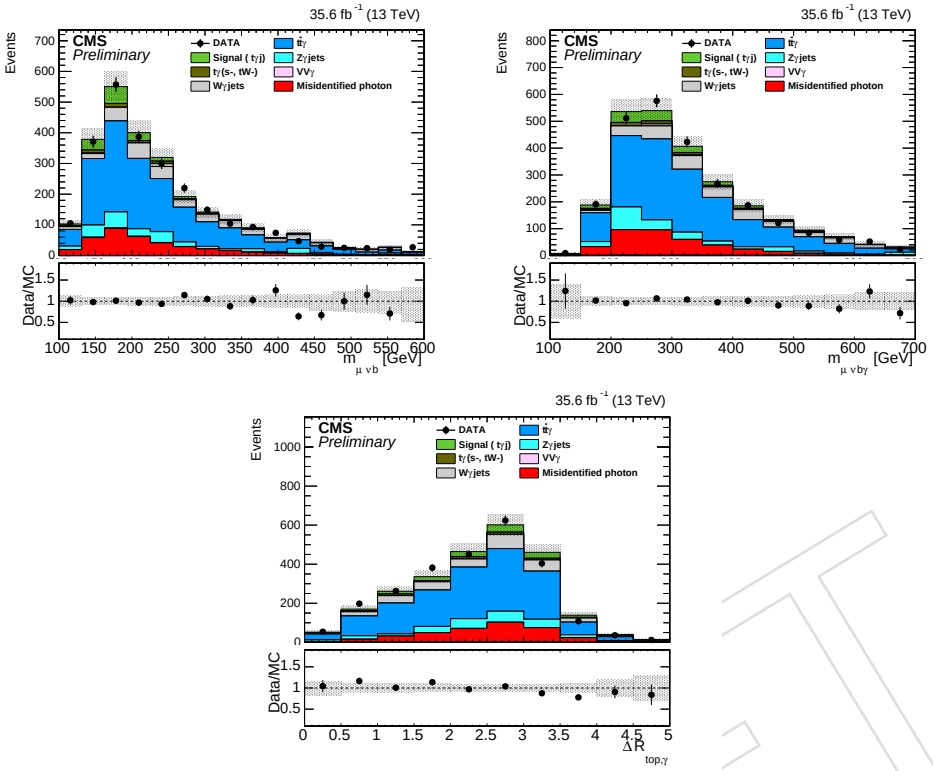

Figure 25: The reconstructed top quark mass, invariant mass of the top quark and photon, and $\Delta R(top, \gamma)$ distributions after all selection criteria.

12 Summary and conclusions

In summary, the production of a single top quark in association with a photon is studied for the first time. The analysis uses data collected by the CMS experiment in pp collisions at the center-of-mass energy of 13 TeV, corresponding to an integrated luminosity of 35.86 fb^{-1}. A multivariate analysis based on kinematic and topological properties of the signal is used to separate the signal from backgrounds and the expected signal is extracted using a maximum-likelihood fit to the distribution of the multivariate discriminant defined with BDT. The expected signal significance is 3.0 standard deviation. The observed signal significance is 4.4 standard deviations and the measured production cross section of $\sigma(t\gamma)\mathcal{B}$ within the kinematic region $E_{T,\gamma} > 25$ GeV, $|\eta| < 1.4442$,and $\Delta R(X, \gamma) > 0.5$ ($X = \mu$,b-jet,light-jet), is $115 \pm ^{+37}_{-32}$(stat $\oplus$ syst) fb which agrees with the standard model prediction value 81 fb.

References

[1] M. Fael and T. Gehrmann, "Probing top quark electromagnetic dipole moments in single-top-plus-photon production", *Phys. Rev.* **D88** (2013) 033003, doi:10.1103/PhysRevD.88.033003, arXiv:1307.1349.

[2] S. M. Etesami, S. Khatibi, and M. Mohammadi Najafabadi, "Measuring anomalous WW γ and t $\bar{\text{t}}\gamma$ couplings using top+ γ production at the LHC", *Eur. Phys. J.* **C76** (2016), no. 10, 533, doi:10.1140/epjc/s10052-016-4376-2, arXiv:1606.02178.

DRAFT

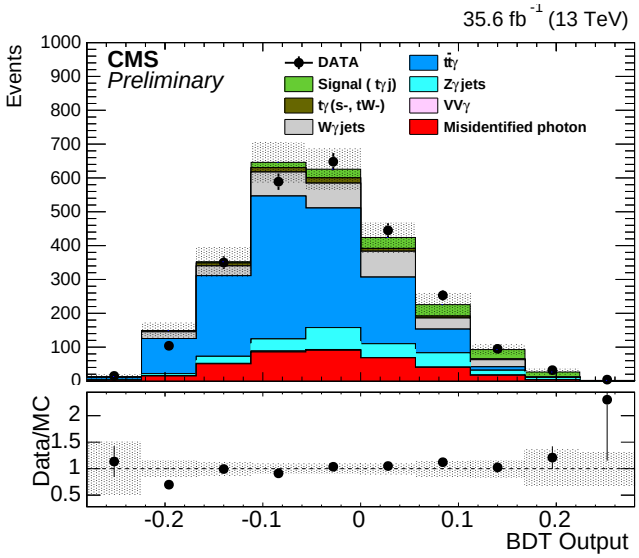

Figure 26: The pre-fit BDT distribution after all selection criteria

[3] CDF Collaboration, "Evidence for $t\bar{t}\gamma$ Production and Measurement of $\sigma_{t\bar{t}\gamma}/\sigma_{t\bar{t}}$", *Phys. Rev.* **D84** (2011) 031104, doi:10.1103/PhysRevD.84.031104, arXiv:1106.3970.

[4] CMS Collaboration, "Measurement of the inclusive top-quark pair + photon production cross section in the muon + jets channel in pp collisions at 8 TeV", Technical Report CMS-PAS-TOP-13-011, CERN, 2013.

[5] ATLAS Collaboration, "Observation of top-quark pair production in association with a photon and measurement of the $t\bar{t}\gamma$ production cross section in pp collisions at $\sqrt{s} = 7$ TeV using the ATLAS detector", *Phys. Rev.* **D91** (2015), no. 7, 072007, doi:10.1103/PhysRevD.91.072007, arXiv:1502.00586.

[6] GEANT4 Collaboration, "GEANT4: A Simulation toolkit", *Nucl. Instrum. Meth.* **A506** (2003) 250–303, doi:10.1016/S0168-9002(03)01368-8.

[7] CMS Collaboration, "CMS Luminosity Measurement for the 2015 Data Taking Period",.

[8] J. Alwall et al., "The automated computation of tree-level and next-to-leading order differential cross sections, and their matching to parton shower simulations", *JHEP* **07** (2014) 079, doi:DOI:10.1007/JHEP07(2014)079, arXiv:1405.0301.

[9] NNPDF Collaboration, "Parton distributions for the LHC Run II", *JHEP* **04** (2015) 040, doi:10.1007/JHEP04(2015)040, arXiv:1410.8849.

[10] T. Sjöstrand, S. Mrenna, and P. Skands, "PYTHIA 6.4 physics and manual", *JHEP* **05** (2006) 026, doi:10.1088/1126-6708/2006/05/026, arXiv:hep-ph/0603175.

[11] CMS Collaboration, "Event generator tunes obtained from underlying event and multiparton scattering measurements", *Eur. Phys. J.* **C76** (2016), no. 3, 155, doi:10.1140/epjc/s10052-016-3988-x, arXiv:1512.00815.

DRAFT

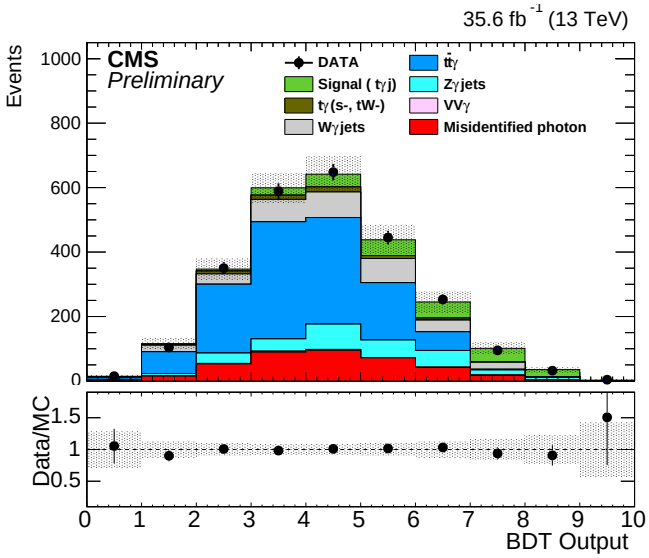

Figure 27: The post-fit BDT distribution after all selection criteria

[12] CompHEP Collaboration, "CompHEP 4.4: Automatic computations from Lagrangians to events", *Nucl. Instrum. Meth.* **A534** (2004) 250–259, doi:10.1016/j.nima.2004.07.096, arXiv:hep-ph/0403113.

[13] S. Frixione, P. Nason, and C. Oleari, "Matching NLO QCD computations with Parton Shower simulations: the POWHEG method", *JHEP* **0711** (2007) 070, doi:10.1088/1126-6708/2007/11/070, arXiv:0709.2092.

[14] CMS Collaboration, "Particle-flow reconstruction and global event description with the CMS detector", arXiv:1706.04965.

[15] *https://twiki.cern.ch/twiki/bin/viewauth/CMS/CutBasedPhotonIdentificationRun2*.

[16] *https://twiki.cern.ch/twiki/bin/view/CMS/MuonPOG*.

[17] *https://twiki.cern.ch/twiki/bin/view/CMS/EgammaPOG*.

[18] M. Cacciari, G. P. Salam, and G. Soyez, "The anti-k_t jet clustering algorithm", *JHEP* **04** (2008) 063, doi:10.1088/1126-6708/2008/04/063, arXiv:0802.1189.

[19] *https://twiki.cern.ch/twiki/bin/view/CMS/JetMET*.

[20] *https://twiki.cern.ch/twiki/bin/viewauth/CMS/JetID*.

[21] CMS Collaboration, "Identification of b-quark jets with the cms experiment", *JINST* **8** (2013) P04013, doi:10.1088/1748-0221/8/04/P04013.

[22] *https://twiki.cern.ch/twiki/bin/viewauth/CMS/BtagRecommendation80XReReco*.

[23] CMS Collaboration, "Measurement of electroweak-induced production of Wγ with two jets in pp collisions at $\sqrt{s} = 8$ TeV and constraints on anomalous quartic gauge couplings", *JHEP* **06** (2017) 106, doi:10.1007/JHEP06(2017)106, arXiv:1612.09256.

DRAFT

[24] CMS Collaboration, "Jet energy scale and resolution in the CMS experiment in pp collisions at 8 TeV", *JINST* **12** (2017), no. 02, P02014, doi:10.1088/1748-0221/12/02/P02014, arXiv:1607.03663.

[25] CMS Collaboration, "Isolated Photon Reconstruction and Identification at 7 TeV", Technical Report CMS-PAS-EGM-10-006, CERN, 2010.

[26] CMS Collaboration, "Measurement of the t t-bar production cross section using events with one lepton and at least one jet in pp collisions at sqrt(s) = 13 TeV", arXiv:1701.06228.

[27] CMS Collaboration, "Measurement of the $t\bar{t}$+γ production cross-section in pp collisions at $\sqrt{s} = 8$ TeV",.

[28] CMS Collaboration, "Measurement of the cross section for electroweak production of $Z\gamma$ in association with two jets and constraints on anomalous quartic gauge couplings in protonproton collisions at $\sqrt{s} = 8$ TeV", *Phys. Lett.* **B770** (2017) 380–402, doi:10.1016/j.physletb.2017.04.071, arXiv:1702.03025.

[29] CMS Collaboration, "Measurement of the W^+W^- cross section in pp collisions at $\sqrt{s} = 8$ TeV and limits on anomalous gauge couplings", *Eur. Phys. J.* **C76** (2016), no. 7, 401, doi:10.1140/epjc/s10052-016-4219-1, arXiv:1507.03268.

[30] CMS Collaboration, "Cross section measurement of t-channel single top quark production in pp collisions at sqrt(s) = 13 TeV", *Submitted to: Phys. Lett. B* (2016) arXiv:1610.00678.

[31] N. Kidonakis, "Theoretical results for electroweak-boson and single-top production", *PoS* **DIS2015** (2015) 170, arXiv:1506.04072.

[32] CMS Collaboration, "Identification of b quark jets at the CMS Experiment in the LHC Run 2", Technical Report CMS-PAS-BTV-15-001, CERN, 2016.

[33] *https://twiki.cern.ch/twiki/bin/viewauth/CMS/MissingETRun2Corrections*.

[34] M. Bahr et al., "Herwig++ Physics and Manual", *Eur. Phys. J.* **C58** (2008) 639–707, doi:10.1140/epjc/s10052-008-0798-9, arXiv:0803.0883.

[35] *https://twiki.cern.ch/twiki/bin/viewauth/CMS/SWGuideHiggsAnalysisCombinedLimit*.

DRAFT